FATIGUE OF HIGH RELATIVE RIB AREA REINFORCING BARS

By
Jun Fei
David Darwin

A Report on Research Sponsored by
THE NATIONAL SCIENCE FOUNDATION
Research Grant No. CMS-9402563

THE U.S. DEPARTMENT OF TRANSPORTATION
FEDERAL HIGHWAY ADMINISTRATION

Structural Engineering and Engineering Materials
SM Report 54

UNIVERSITY OF KANSAS CENTER FOR RESEARCH, INC.
LAWRENCE, KANSAS
July 1999

ABSTRACT

The fatigue performance of high relative rib area reinforcing bars is compared to that of conventional bars. Fatigue tests involve No. 4 (13mm) and No. 5 (16mm) bars with relative rib areas (ratio of projected rib area normal to bar axis to the product of the nominal bar perimeter and the center-to-center rib spacing) ranging from 0.064 to 0.146. The tests include 69 specimens representing 6 deformation patterns [2 for No. 4 (13mm) bars and 4 for No. 5 (16mm) bars] to investigate the effect of deformation pattern on fatigue behavior. The tests were conducted in air using stress ranges of 20, 25, 30, and 35 ksi (138, 172, 207, and 241 MPa) with a minimum stress of zero. Characteristics of fatigue crack zones and the details of lug geometry are provided.

The test results indicate that the stress range, bar diameter, and surface geometry, especially the lug base radius-to-height ratio (r/h), have significant effects on the fatigue strength of the bars. Fatigue strength and fatigue life decrease with increased stress range and bar diameter and decreased r/h ratio. Relative rib area has no effect on fatigue performance.

Keywords: concrete; deformation pattern; fatigue; reinforcing bars; relative rib area

ACKNOWLEDGEMENTS

This report is based on a thesis submitted by Jun Fei in partial fulfillment of the requirements of the M.S.C.E. degree. Support for this research was provided by the National Science Foundation under NSF Grant No. CMS-9402563, the U.S. Department of Transportation – Federal Highway Administration, the Lester T. Sunderland Foundation, ABC Coating, Inc., AmeriSteel (formerly Florida Steel Corporation), Birmingham Steel Corporation, Chaparral Steel, DuPont Powder Coatings, Fletcher Coating, North Star Steel Company, and 3M Corporation. Additional support was provided by Geiger Ready-Mix, Iron Mountain Trap Rock Company, and Dayton Richmond.

TABLE OF CONTENTS

	Page
ABSTRACT	i
ACKNOWLEDGEMENTS	ii
LIST OF TABLES	v
LIST OF FIGURES	vi
CHAPTER 1: INTRODUCTION	1
1.1 General	1
1.2 Previous Work	3
1.3 Object and Scope	12
CHAPTER 2: EXPERIMENTAL WORK	13
2.1 Overview of Experimental Program	13
2.2 Test Specimen	13
2.3 Specimen Preparation	16
2.4 Test Procedure	17
2.5 Test Results	19
CHAPTER 3: EVALUATION AND DISCUSSION OF TEST RESULTS	23
3.1 General	23
3.2 Effect of Bar Diameter	23
3.3 Effect of Surface Geometry	24
3.4 Effect of Relative Rib Area	25
3.5 Comparison with Previous Test Results in Air	27
3.6 Comparison with AASHTO Fatigue Design Criteria	28
CHAPTER 4: SUMMARY AND CONCLUSIONS	31
4.1 Summary	31
4.2 Conclusions	31
REFERENCES	33
TABLES	36
FIGURES	47
APPENDIX	76

LIST OF TABLES

		Page
Table 2.1	Deformation Properties of Reinforcing Bars	36
Table 2.2	Rib Heights of Transverse Deformations on Bars Investigated	37
Table 2.3	Mechanical Properties of Reinforcing Bars	39
Table 2.4	Stresses Introduced by Gripping System	40
Table 2.5	Fatigue Test Results of Reinforcing Bars	41
Table 2.6	Measurements of Lug Properties Obtained with Scanning Electron Microscope	45

LIST OF FIGURES

		Page
Fig. 2.1	Test Bars	47
Fig. 2.2	Schematic Illustration of Relative Rib Area (see Eq. 2.1)	48
Fig. 2.3	Typical Stress-Strain Curve for Ch4S60 Bars	49
Fig. 2.4	Typical Stress-Strain Curve for SMI4S60 Bars	50
Fig. 2.5	Typical Stress-Strain Curve for Ch5S60 Bars	51
Fig. 2.6	Typical Stress-Strain Curve for Ch5S Bars	52
Fig. 2.7	Typical Stress-Strain Curve for N5S Bars	53
Fig. 2.8	Typical Stress-Strain Curve for FK5S60 Bars	54
Fig. 2.9	Specimen prepared for Fatigue Tests	55
Fig. 2.10	Schematic of Test Set-Up	56
Fig. 2.11	S-N Curves for No. 4 (13 mm) Bars	57
Fig. 2.12	S-N Curves for No. 5 (16 mm) Bars	58
Fig. 2.13	Fatigue Crack Surfaces on Ch4S60 Bars	59
Fig. 2.14	Fatigue Crack Surfaces on SMI4S60 Bars	60
Fig. 2.15	Fatigue Crack Surfaces on Ch5S60 Bars	61
Fig. 2.16	Fatigue Crack Surfaces on Ch5S Bars	62
Fig. 2.17	Fatigue Crack Surfaces on N5S Bars	63
Fig. 2.18	Fatigue Crack Surfaces on FK5S60 Bars	64
Fig. 2.19	Scanning Electron Microscope Image of a Lug on a Ch4S60 Bar	65
Fig. 2.20	Scanning Electron Microscope Image of a Lug on a SMI4S60 Bar	66
Fig. 2.21	Scanning Electron Microscope Image of a Lug on a Ch5S60 Bar	67

LIST OF FIGURES (continued)

		Page
Fig. 2.22	Scanning Electron Microscope Image of a Lug on a Ch5S Bar	68
Fig. 2.23	Scanning Electron Microscope Image of a Lug on a N5S Bar	69
Fig. 2.24	Scanning Electron Microscope Image of a Lug on a FK5S60 Bar	70
Fig. 3.1	Effect of Bar Diameter	71
Fig. 3.2	Effect of Critical r/h Ratios	72
Fig. 3.3	Effect of Average w/h Ratios	73
Fig. 3.4	Effect of the Sharpest Average Flank Angles	74
Fig. 3.5	Effect of Relative Rib Area (R_r) Values	75

CHAPTER ONE

INTRODUCTION

1.1 General

The requirements for reinforcing bar deformation patterns used in the United States, given in ASTM A 615/615M, A 616/616M, A 617/617M, and A 706/706M, were established over fifty years ago based on work by Clark (1946, 1949). Although a great deal has been learned about the behavior of reinforced concrete members in the interim, no changes have been made in those requirements.

Work has been under way at the University of Kansas since 1991 to determine if the development characteristics of reinforcing bars can be improved by modifying the bar deformation pattern. Early in the study, Darwin and Graham (1993a, 1993b) demonstrated that, for uncoated reinforcement, the higher the relative rib area, R_r (ratio of projected rib area normal to bar axis to the product of the nominal bar diameter and the center-to-center rib spacing), the higher the bond strength between reinforcing bars and concrete, if the bars are confined by transverse reinforcement. If not confined, the bond strength of bars without epoxy coating is insensitive to the specific combination of rib height and spacing. Darwin et al. (1995, 1996) also found that epoxy-coating is less detrimental to the bond strength of high relative rib area bars than to the bond strength of conventional bars, whether or not the bars are confined by transverse reinforcement. As a result, the maximum development length modification factor used for high relative rib area epoxy-coated bars could be reduced by 20 percent compared to current requirements. To date, however, there is no data available on the fatigue performance of high relative rib area bars. Of particular concern is the effect of closer and/or higher ribs on fatigue performance.

The phenomenon of weakening of a material as the result of repeated loads is called fatigue (ACI Committee 215 1974). Fatigue is a process by which cracks initiate and then

propagate under cyclic loading in a structural member, resulting in damage or complete fracture of the member. The magnitude of loading required to produce fatigue failure may be much less than that needed to fail the material with a single application of load. Fatigue strength is defined as the greatest stress which can be sustained for a given number of stress cycles without failure (ACI Committee 215 1974). However, for design purposes, fatigue strength is usually defined as the stress *range* a material can sustain without failure for a specific number of cycles (Narayanaswamy et al. 1977).

Fatigue is not a major consideration in the design of most reinforced concrete structures. To date, there have been no fatigue fractures reported for concrete structures under normal service loading. However, reinforced concrete is widely used in bridges, offshore structures, and machine foundations. These structures are subjected to time-dependent oscillatory loads that result from vehicles, strong wave and wind action, and dynamic loading from machines. The stresses due to these loads may cause fatigue in the structures and result in premature failure.

Extensive research on the fatigue strength of conventional deformed bars has been conducted over the years. Fatigue loading considerations for the United States are reviewed by ACI Committee 215 (1974) and Helgason et al. (1976). Extensive data exists on the fatigue characteristics of conventional reinforcing bars (values of R_r between 0.060 and 0.085) tested both in concrete and in the air. That data has been used to establish the AASHTO requirements on fatigue (AASHTO *Standard Specifications for Highway Bridges*, 1996). No information, however, has been obtained on the fatigue behavior of the deformed bars with high relative rib areas. Since bars with new deformation patterns and high relative rib areas can be used under the provisions of ACI T2.1-98, there is a need to understand the fatigue behavior of these bars.

This report describes fatigue tests of commercially produced No. 4 (13 mm) and No. 5 (16 mm) reinforcing bars with relative rib areas ranging from 0.064 to 0.146. The test results show that fatigue behavior is insensitive to the relative rib area, but depends on the bar

surface geometry, especially the lug base radius-to-height (r/h) ratio. Observations on the location of crack initiation and characteristics of the fatigue failure surface are presented. Details of test specimen preparation and gripping method, the greatest difficulty involved in fatigue testing in air, are also provided.

1.2 Previous Work

Since the early 1950's, considerable research has been performed on the fatigue behavior of deformed and plain reinforcing bars, alone or embedded in concrete, especially in North America, Europe, and Japan. This research has provided valuable information on the factors that influence the fatigue behavior of reinforcing bars.

Pfister and Hognestad (1964) studied the fatigue behavior of reinforcing bars embedded in concrete. The study covered three grades and four deformation patterns and included 181 reinforced concrete beams with straight or cold bent bars. They found that yield strength, test beam cross section, and minimum stress level do not significantly affect the fatigue strength of bars up to 2 million cycles. However, the fatigue strength for one deformation pattern was 35 percent lower than that of another, indicating that surface geometry has a strong effect on the fatigue performance. They also observed that the fatigue strength of bars cold bent to 45 degrees was only 50 percent of that of straight bars. By examining the locations where the fatigue cracks initiated, they concluded that all fatigue cracks initiate at the root of a lug.

Burton (1965) reported the results of fatigue tests on reinforcing bars embedded in concrete. The tests were conducted using three stress ranges, 31, 35 and 39 ksi (214, 241, and 269 MPa), with a minimum tensile stress of 5 ksi (35 MPa), on concrete beams reinforced with a single No. 8 (25 mm) reinforcing bar conforming to ASTM A 15 for grade and A 305 for the deformations. One deformation pattern produced by fresh rolls, partially worn rolls, or fully worn rolls at the time of manufacture, was used. The longitudinal ribs were placed in a horizontal plane (perpendicular to the plane of flexure) in half of the beams, and vertically in the remainder. A total of thirty six 8 in. wide by 14 in. deep (203 mm by 356 mm) beams

were tested. Three major variables, position of the longitudinal ribs, surface geometry due to different condition of the rolls at the time of manufacture, and stress range were investigated. From the test results, Burton reported that stress range is the primary factor influencing fatigue strength. As the stress range increases, fatigue strength decreases. The maximum stress concentration occurred at the junction between the transverse and longitudinal ribs instead of at the root of a lug. Burton also concluded that conditions of wear for the rolls had a minor effect on the fatigue life of the bars in his study.

McDermott (1965) performed fatigue tests on No. 4 and No. 11 (13 and 36 mm) A 432 reinforcing bars with the DI-LOK pattern (the transverse ribs crossed midway between the two longitudinal ribs and met at the longitudinal rib - often referred to as an X-pattern). The No. 4 and No. 11 (13 and 36 mm) bars had average yield strengths of 69.8 and 66.3 ksi (481 and 457 MPa) and average tensile strengths of 109.9 and 100.4 ksi (757 and 692 MPa), respectively. The tests were conducted under axial loading in air with a stress ratio (ratio of minimum stress to maximum stress in a load cycle) between zero and ±0.03. McDermott concluded that the fatigue strength was about 39 ksi (269 MPa) corresponding to 3 million cycles for the No. 4 (13 mm) bars and about 19 ksi (131 MPa) corresponding to 6 million cycles for the No. 11 (36 mm) bars. He explained the size effect by the fact that the No. 4 (13 mm) bars had a smoother transition between the transverse lug and the barrel of the bar. He found that fatigue cracks initiate at the intersection of the transverse and longitudinal deformations or at the intersection of two transverse lugs. The test results suggested that using a fillet rather than a sharp angle at the root of a lug and tapering (gradually terminating) the transverse deformations before they meet the longitudinal ribs will increase fatigue strength. He also described the procedures used for preparing the bar and gripping the bar during the test, which included complete removal of the transverse ribs in the regions in which the bars were gripped.

Hanson, Burton, and Hognestad (1968) described the effect of deformation pattern on the fatigue behavior of No. 8 (25 mm) reinforcing bars in concrete beams. American-made bars

(Series I) had crescent-shaped transverse lugs, while European-made bars (Series II) had inclined transverse lugs. All of the bars had transverse lugs that did not merge into the longitudinal ribs. The beams were 8 in. wide and 14 in. deep (203 mm by 356 mm) reinforced with one No. 8 (25 mm) bar. Fourteen beams in Series I and 12 beams in Series II were tested. They found that the fatigue strengths corresponding to 2 million cycles for Series I and Series II bars were 26 ksi and 37.5 ksi (179 and 258 MPa), respectively. By comparing the results with previous tests of American-made bars with transverse lugs that merge into the longitudinal ribs, they found that fatigue strength is not necessarily improved by terminating the transverse lugs before they meet the longitudinal rib, in contradiction to the conclusion by McDermott (1965). They observed that fatigue cracks initiated at the base of the crescent-shaped lugs in the Series I bars and adjacent to the sharp side of a lug (the side with the smaller radius at the root of the lugs) in the Series II bars. The fracture surface of Series I bars was a plane normal to the axis of the bar, while the fracture surface of Series II bars was a plane inclined at an angle of about 45 degrees with the axis of the bar.

McDermott (1969) studied the fatigue characteristics in air of No. 8 (25 mm) A 615 Grade 60 reinforcing bars with different deformation patterns. Bars with the DI-LOK pattern, bars with seven different experimental patterns, and four domestic competitors' bars were included in the program. All tests were conducted under zero-to-tension axial load. Sinusoidal load variation was selected, with a frequency of 7 Hz. The purpose of the tests was to find the best deformation pattern for further development. From the test results, McDermott found that bars with a four-start-helix transverse deformation pattern (a long-pitch spiral pattern in which a transverse cross-section of the bar crosses four transverse deformations) had the best fatigue behavior of the bars tested. By examining the details of the deformation patterns, McDermott found that decreasing the angle between the transverse lug and the longitudinal rib and avoiding the intersection of two transverse deformations results in an increase in fatigue strength. This report also described test specimen preparation. The deformations were only partially removed from the end portions of the bar, instead of

completely machined off as described in his 1965 report, to avoid removing too much of the cross-sectional area in the grip region. At both ends of the specimen, he used copper tubing with fine white sand bonded to the inside surface with USS Nexus adhesive S-7001.

McDermott (1971) provided more information on the fatigue behavior of the four-start-helix bars described in his 1969 report and compared the fatigue behavior of the helix bars with that of the DI-LOK bars in his 1965 report. In this report, the fatigue strength corresponding to 4 million cycles for No. 10 (32 mm) and No. 4 (13 mm) helix bars were 29 ksi and 37.5 ksi (200 and 258 MPa), respectively. He observed that larger bars had lower fatigue strength and explained it by the notch effect resulting from surface imperfections at the ribs, which are more pronounced in the larger bars. McDermott concluded that the No. 10 (32 mm) helix bars had better fatigue performance than the No. 11 (36 mm) DI-LOK bars (McDermott 1965). The No. 4 (13 mm) helix bars, however, do not appear to behave quite as well as the earlier No. 4 (13 mm) DI-LOK bars. In general, he felt that the results for larger bars can be conservatively applied to all bars and used as the basis for design criteria. Overall, McDermott confirmed his 1969 conclusions that the fatigue characteristics of the four-start-helix deformation pattern are superior to those of the DI-LOK pattern. The test specimen preparation was the same as that described in his 1969 report except that this time he used copper tubing only, instead of using the copper tubing with sand bonded to the inside surface.

MacGregor, Jhamb, and Nuttall (1971) reported the fatigue behavior of No. 5 (16 mm), No. 8 (25 mm), and No. 11 (36 mm) hot rolled deformed bars with nominal yield strengths of 40, 60, and 75 ksi (276, 413, and 517 MPa). The study included 72 flexural fatigue tests on reinforced concrete beams containing one deformed bar and 36 standard rotating beam fatigue tests on plain specimens machined from the bars. They observed that the fatigue strength of the hot rolled deformed bars ranged from 29 to 37 ksi (200 to 255 MPa), at 5 million cycles, but was independent of grade. In contrast, the fatigue strength of the specimens machined from the center of the deformed bars increased linearly with an increase

of the tensile strength of the bar. They explained the different effects of bar grade on the fatigue strength of deformed bars and plain specimens by the stress concentrations at the base of the deformations and the presence of a relatively low strength decarburized layer on the outside of all the deformed bars. They also observed that larger bars had lower fatigue strength and that fatigue cracks originated at the base of a transverse lug or at the point where a transverse lug merged into a longitudinal rib.

Hanson, Helgason, and Ball (1972) studied the fatigue behavior of Grade 60 No. 8 (25 mm) bars on which the transverse lugs, inclined at an angle of about 45 degrees to the bar axis, form helixes around the bar. Their investigation consisted of 24 fatigue tests of bars embedded in T-shaped reinforced concrete beams. The minimum stress was 6 ksi (41MPa) tension throughout the tests. Based on the test results, they concluded that the mean stress range causing fatigue failure in 5 million cycles was 27.8 ksi (192 MPa). They examined the fracture surface and found that 60 percent of the cracks began at the base of transverse lugs, while the other cracks began at the edge of the bar identification marks.

Jhamb and MacGregor (1974a) studied the effect of surface geometry on the fatigue of reinforcing bars. Their study included 88 No. 8 (25 mm) bar specimens and 32 plain machined bar specimens tested in air under repeated axial loading to determine the effects of the deformations, decarburization of the bar surface, rust and mill scale, and grade of steel. They concluded that there is a significant decrease in fatigue strength due to the presence of deformations and decarburization of the bar surface. Rust and mill scale do not influence fatigue strength. The grade of steel had no influence on the fatigue strength of the deformed bars, while specimens machined from the center of deformed bars showed a linear increase in fatigue strength with the grade, matching the results of their 1971 report. They also observed that the fatigue strength of bars tested in air was lower than that of bars tested in concrete beams. Examining the fracture surface of the deformed bars, they found that the fatigue failures originated at the base of a transverse lug. The fatigue fracture zone was a smooth surface surrounded by a rough and crystalline tension fracture zone.

Jhamb and MacGregor (1974b) also studied the stress concentrations on the surface of deformed bars. Typical hot rolled deformed reinforcing bars contain two longitudinal ribs and a regular pattern of equally spaced transverse lugs, which cause stress concentrations. In 1974, there were no published values for stress concentration factors K_T that represented the stresses at the bases of deformations. They determined the values of K_T using finite element analysis and a 30-inch (762 mm) No. 8 (25 mm) specimen with electrical resistance strain gages. Based on the study, Jhamb and MacGregor concluded that the ratio of the lug base radius (r) to the lug height (h) has the most pronounced effect on K_T. The values of K_T decrease with an increase in r/h value. The fatigue strength of the deformed bars decreases when the ratio of radius to lug height r/h is less than about 1.25 and is almost constant for r/h ratios greater than 1.25.

Helgason, Hanson, Somes, Corley, and Hognestad (1976) studied the behavior of Grade 60 reinforcing bars in test programs designed to permit a valid statistical appraisal of the factors that effect fatigue performance. The tests included 353 concrete beams, each containing a single straight test bar as the main reinforcement. The major test variables were stress range, minimum stress level, bar diameter, grade and surface geometry, and effective beam depth. They observed that: (1) The stress range of the load cycle is the predominant factor determining the fatigue life of the bar. There exists a limiting stress range, the fatigue limit, above which a reinforcing bar is certain to fracture in fatigue and below which a reinforcing bar may be able to sustain a virtually unlimited number of cycles. (2) For the same stress range, the minimum stress level of a stress cycle has a significant effect on fatigue strength in the finite-life region of the bars. An increase in the tensile minimum stress (and, thus, an increase in the maximum stress) was found to result in a decrease in fatigue strength. Fatigue strength was found to increase with an increasing compressive (more negative) minimum stress. (3) Bar diameter and grade of bar were found to influence the finite-life fatigue strength of reinforcing bars. Larger size bars have lower fatigue strength, while higher grade bars have increased fatigue strength. The conclusion about the effect of

grade of steel on fatigue strength is in contradiction to the conclusions of MacGregor, Jhamb, and Nuttall (1971) and Jhamb and MacGregor (1974a). (4) Transverse lugs and manufacturer's bar identification marks cause stress concentrations at their juncture with the barrel of a bar. The magnitude of a stress concentration is primarily related to the ratio of the radius at the base of the deformation to its height. By examining the fracture surface, they observed that fatigue fractures initiate at the base of a transverse lug or a bar mark. Fatigue cracks propagate radially from the point of initiation in a direction perpendicular to the axis of a bar. The relatively smooth, dull-appearing fatigue crack zone is surrounded by a rough, crystalline tension fracture zone. Fatigue crack growth is most rapid near the end of the fatigue life. Based on the test results and the statistical analysis, they provided an equation for the design of flexural reinforcement in concrete members subjected to cyclic loading. The equation is: $f_r = 21 - 0.33f_{min} + 8$ (r/h), where f_r = stress range (ksi), f_{min} = minimum stress (ksi), r/h = ratio of base radius to rib height; if r/h is not known, a value of 0.3 can be used.

Narayanaswamy, Gupta, Chhauda, and Rajaraman (1977) studied the fatigue behavior of Indian made cold-worked deformed bars. The bars had four longitudinal ribs and crescent-shaped transverse deformations. Their tests included 8 concrete beams with a 300 mm wide by 350 mm (12 in. by 14 in.) deep cross-section, reinforced with one 25 mm (No. 8) bar at the bottom of the beam. The stress range corresponding to 2 million loading cycles was 240 MPa (35 ksi), a result comparable to bars of similar type and grade made in Europe. They also examined the fatigue fracture surface and observed that the point of crack initiation is at the root of the transverse lugs or longitudinal ribs (the reasons for crack initiation for the latter case is not clear). By applying a factor of safety of 1.4, they recommended a permissible stress range value of 171.5 MPa (24.8 ksi) for the design of reinforced concrete members subjected to repeated loading.

Moss provided information (1980) on the fatigue of British high-yield reinforcing bars tested in air for use in updating BS5400, which concerned the design of bridges. Continuous and butt-welded specimens using high-yield reinforcing bars were included in his test. The

experimental relationship between stress range and fatigue life for continuous bars had the same form as the design curves incorporated in BS5400 at that time. The fatigue performance of reinforcing bars was reduced by the presence of a butt weld. Moss observed that larger bars were significantly less resistant to fatigue damage than smaller bars of the same type. Examining the fracture surface, he found that fatigue cracks in continuous bars initiate at small defects associated with the surface oxide layer and that the rib pattern on deformed bars has little influence on the point of fatigue crack initiation. His observations do not match earlier conclusions for U.S. bars that fatigue cracks start at the root of a transverse lug, at the intersection between a transverse lug and a longitudinal rib, at the intersection of two transverse lugs, or at the root of identification marks. (Pfister and Hognestad 1964, McDermott 1965, Hanson, Burton, and Hognestad 1968, Hanson, Helgason, and Ball 1972, Helgason, Hanson, Somes, Corley, and Hognestad 1976)

Matsumoto (1988) studied the fatigue characteristics of reinforcing bars in air and the effect of cold-work (pre-strain) on fatigue strength. His experiments included two phases, both using axial-tension fatigue tests on Grade 60 No. 3 (9.53 mm) straight bars. Fatigue tests were conducted on 28 specimens to obtain the S-N curves for normal bars in Phase I. Nine different stress ranges of constant-amplitude sinusoidal load (10 Hz) with 6 ksi (41 MPa) minimum stress were used in this phase. In Phase II, 8 specimens were used to investigate the effect of cold-work (pre-strain) on fatigue behavior, using a stress range and minimum stress of 42 and 6 ksi (289 and 41 MPa), respectively. With the test results, Matsumoto found that the fatigue strength of Grade 60 No. 3 (9.53 mm) normal bars was 32 ksi (221 MPa) corresponding to 2 million cycles. The fatigue strength of prestrained (cold-worked) bars was lower than that of the normal bars by 15 percent or less.

Zheng and Abel (1998) used finite element analysis to investigate stress concentrations on the surface of bars. They constructed two models to simulate transverse lug patterns. Model I simulated equally spaced transverse lugs, where each lug is relatively far away from its neighbors. Model II simulated bars with unequally spaced lugs distributed in a way that a

lug is closer to its neighbor on one side but distant from its other neighbor. The results from Model I showed that stress concentrations exist only in a very small area in the vicinity of the root of a lug and that the greatest stress is at the junction between the root of the transverse lug and the base material. From Model II, they found that when the distance between two neighboring lugs decreases, the stress concentration factor increases at the inner side of the lugs and reaches a maximum value of 2.65 when two lugs merge. Zheng and Abel concluded that the lug base radius-to-height ratio (r/h) is the primary factor influencing the stress concentrations. An increase in the r/h ratio results in a decrease in stress concentrations and, therefore, an increase in fatigue strength. Lug width-to-height ratio (w/h) and flank angles have minor effects on the stress concentrations. Decreased w/h ratios and flank angles result in decreased stress concentrations and, thus, an increase in fatigue strength. They also observed that the stress concentration of bars with transverse lugs normal to the bar axis is higher than that of bars with transverse lugs at an angle to the bar axis.

Thandavamoorthy (1999) studied the fatigue of quenched and tempered bars embedded in concrete beams. The bars have low carbon content and are manufactured using the Tempcore or Thermex process, in which bars are quenched with water after hot rolling, resulting in a tough outer layer of tempered martensite (with residual compressive stress) and a core of ferrite-pearlite (with residual tensile stress). The bars have greater ductility than conventional bars. Eight concrete beams with a 150 x 300 mm (6 x 12 in.) cross-sections were tested to verify whether the bars can resist the safe stress range for 2 million cycles determined with the relationship $f_r = 21 - 0.33f_{min} + 8(r/h)$ (ksi) [$f_r = 145 - 0.33f_{min} + 55(r/h)$ (MPa)] (Helgason et al. 1976) which is now recommended by ACI Committee 343 on Bridge Structures (1991) and required by the AASHTO Bridge Specifications (1996). The beams were subjected to sinusoidal constant amplitude loading at 5 Hz (two beams) and 10 Hz (six beams). Four were under three-point bending and the other four were under four-point bending. All of the beams sustained the designated stress range without failure for over 2

million cycles. Thandavamoorthy concluded that the test results indicated that the fatigue strength of these bars is comparable to the fatigue strength of conventional bars.

Zheng and Abel (1999) also studied the fatigue performance of Tempcore bars. In contrast to Thandavamoorthy's (1999) tests, all of the bars in this study were tested under axial loading in air instead of being embedded in concrete. Seven different diameters, ranging from 12 mm to 36 mm (No. 4 to No. 11), with 400 MPa (58 MPa) nominal yield strength were used in the program. The minimum stress level was 0 ksi. Based on the test results, Zheng and Abel concluded that the fatigue behavior of the Australian-made Tempcore bars is superior to that of conventional high-strength bars.

1.3 Object and Scope

The purpose of this research is to compare the fatigue behavior of conventional and high relative rib area reinforcing bars. Relative rib areas range from 0.064 to 0.146. This report is also intended to provide information that will serve as a guide for preparing and testing small diameter bars subjected to fatigue loading in air. Stress range-fatigue life curves, commonly referred to as S-N curves, are obtained for the bars. In this study, four stress ranges [20, 25, 30, 35 ksi (138, 172, 207, and 241 MPa)] with 0 minimum stress level, two bar sizes [No. 4 and No. 5 (13 and 16 mm)], and 6 deformation patterns (Ch4S60, SMI4S60, Ch5S60, Ch5S, N5S, and FK5S60) are used to evaluate the effects of stress range, bar diameter, surface geometry, and relative rib area on the fatigue behavior of bars. The characteristics of the fatigue crack surface and locations of the fatigue crack initiation are examined.

Chapter 2 presents the properties of the reinforcing bars, the test specimen preparation, the test procedures, and the test results. Chapter 3 presents the evaluation and discussion of the test results. Chapter 4 summarizes the research effort and presents the conclusions.

CHAPTER TWO

EXPERIMENTAL WORK

2.1 Overview of Experimental Work

The experimental program described in this report consisted of 69 fatigue tests of Grade 60 No. 4 (13 mm) and No. 5 (16 mm) reinforcing bars with relative rib areas ranging from 0.064 to 0.146. All of the tests were conducted in air under cyclic axial loading. The minimum stress level was 0 ksi. The tests included 21 No. 4 (13 mm) bar specimens, 9 Ch4S60 bars and 12 SMI4S60 bars, and 48 No. 5 (16 mm) bars, 12 each of four patterns, Ch5S60, Ch5S, N5S, and FK5S60. The bars are shown in Fig. 2.1.

The key parameters in the study are stress range (difference between the maximum and minimum stress in a load cycle), bar size [No. 4 or No. 5 (13 mm or 16 mm)], surface geometry, and relative rib area (0.064 to 0.146).

Four nominal stress ranges [20, 25, 30, and 35 ksi (138, 172, 207, and 241 MPa)] were used. Bars that sustained 2 million cycles without breaking were considered to be loaded below their fatigue strength (the greatest stress range under which a bar can sustain virtually an unlimited number of cycles without failure). S-N curves, representing the relationship between the stress range (S) and the number of cycles (N), were obtained. Detailed surface geometries were measured and characteristics of the fatigue cracks were examined.

2.2 Test Specimens

The reinforcement used in this program included Grade 60 No. 4 (13 mm) and No. 5 (16 mm) bars with relative rib areas ranging from 0.064 to 0.146. The calculation of relative rib area, R_r, is illustrated in Fig. 2.2. For the purposes of this study,

$$R_r = \frac{h_r}{s_r}\left(1 - \frac{\sum gaps}{p}\right) \qquad (2.1)$$

where h_r = average height of deformations, in. or mm (explained below)

s_r = average spacing of deformations, in. or mm

$\sum gaps$ = sum of the gaps between ends of transverse deformations, plus the width of any continuous longitudinal lines used to represent the grade of the bar multiplied by the ratio of the height of the line to h_r, in. or mm

p = nominal perimeter of the bar, in. or mm

Two No. 4 (13 mm) bars with MIM (Manufacture Identification Marks) Ch4S60 and SMI4S60 and 4 No. 5 (16 mm) bars with MIM Ch5S60, Ch5S, N5S, and FK5S60 were used. The SMI4S60 (R_r = 0.064), N5S (R_r = 0.076), and FK5S60 (R_r = 0.088) were conventional bars, while the Ch4S60 (R_r = 0.128), Ch5S60 (R_r = 0.146), and Ch5S (R_r = 0.100) were high relative rib area bars. The FK5S60 bar is a Thermex bar, and the other bars are hot rolled bars.

The Ch4S60, SMI4S60, Ch5S60, and FK5S60 bars had two longitudinal ribs, while the Ch5S and N5S bars had two main longitudinal ribs and an additional rib, indicating the bar grade. All of the bars had equally spaced transverse deformations (also referred to as ribs or lugs). The transverse lugs on the SMI4S60 and FK5S60 bars were normal to the bar axis, while the transverse lugs of the other four bars were at an angle to the bar axis.

The deformation measurements of bars are summarized in Table 2.1. The transverse rib height measurements used for calculating R_r are given in Table 2.2. The rib heights shown in Table 2.2 were measured using a Starrett dial gage with a 0.01 mm least reading. To match the other measurements, the rib heights are changed from millimeters in Table 2.2 to inches in Table 2.1.

A sample of a bar, about three feet long, was selected and cleaned with a dry cloth to remove dust to prepare for the rib height, rib spacing, and gap widths measurements. The rib heights were measured at five locations, evenly distributed along the length of the bar. At each location, the rib heights were measured at ten points around the bar perimeter (Table 2.2). The dial gage had a pointed tip to measure the rib heights. At each point, the rib height is taken as the difference between measurements at the top of the rib and the barrel of the bar (midway between the measured rib and an adjacent rib). The average rib height h_r at each location is a weighted average. The heights measured at the four points at the base of the longitudinal ribs are weighted at one-half of the heights of the other six points [(0.5(A+E+F+J)+(B+C+D+G+H+I))/8 Table 2.2]. The average rib height shown in Table 2.1 represents the average of the 5 locations. This value is slightly different from the ASTM average, which is based on three measurements per deformation, one at the center of the overall length and the other two at the quarter points of the overall length (ASTM 615).

The center-to-center rib spacing and gap width for the longitudinal ribs were measured using a Peacock caliper with a 0.001 in. least reading. The average rib spacing was determined by measuring the distance between the faces of two widely separated ribs and divided by the number of ribs within the distance. Gap widths are determined at the points where the longitudinal ribs meet the barrel of the bar. The gap width measurements were taken at five locations (at least 3 ribs between two adjacent locations) along each longitudinal rib. When a bar, such as Ch5S or N5S, had an extra longitudinal rib indicating the bar grade, the height and width of that rib were also measured. The height was determined by taking the difference between a measurement at the top of the rib and the average of measurements on both sides of the rib where it meets the barrel of the bar. The width was measured similar to gap width. Measurements on extra longitudinal ribs were taken midway between transverse ribs at five locations along the bar.

The mechanical properties of the bars were obtained using standard tension tests on three specimens for each type of bar. The results are given in Table 2.3. Typical stress-strain

curves for Ch4S60, SMI4S60, Ch5S60, Ch5S, N5S, and FK5S60 bars are shown in Figs. 2.3-2.8. All bars met the requirements of ASTM A 615.

The fatigue test specimens were designed to fit the testing machine grips and provide a test section length of at least five-bar diameters. The No. 4 (13 mm) and No. 5 (16 mm) bars, had lengths of 12 inches and 13 inches (305 and 330 mm), respectively.

2.3 Specimen Preparation

Compared with fatigue tests of bars in concrete, tests of bars in air are cheaper, quicker and easier to perform. However, establishing a technique for gripping the bars in the testing machine can be difficult because the combination of the gripping force and the fatigue loading may cause the test specimen to fail in the grip instead of in the test section. No standard testing method has been established to determine the fatigue strength of deformed reinforcing bars in the United States. Based on previous work, especially the techniques developed by McDermott (1969 and 1971) and experience gathered from the pilot tests, a procedure for specimen preparation was established. Specimens prepared using this procedure are illustrated in Fig. 2.9.

All of the specimens were free of manufacture's identification marks because their effect on the fatigue behavior of reinforcing bars is not considered in this study. Specimen preparation involved machining the bars to partially remove the deformations, with a tapered transition, at both ends of the bar. The tapered transition was introduced because it provided a gradual and smooth surface change, thus, reducing the possibility of the introduction of a stress concentration due to specimen preparation. The deformations were not completely removed because complete removal reduced the cross-sectional area enough to cause the specimen to break and made the bar difficult to grip. The higher gripping pressure needed to prevent the bar from slipping caused the bar to break in the grips. After the bars were machined, the ends of the bars were shot peened. The central portion of the bar was protected during this operation by wrapping with multifold paper towels and UT-602 electrical tape. As

described below, fatigue failure of a bar in its central portion was considered satisfactory. The Ch4S60, Ch5S60, Ch5S, and N5S bars were shot peened using 90 psi (620 kPa) air pressure with steel shot (4 minutes per end) at a commercial facility in Topeka, Kansas. The FK5S60 bars were shot peened using 70-80 psi (482-551 kPa) air pressure with steel shot (10 minutes per end) at the University of Kansas. The SMI4S60 bars did not require preparation and were tested directly after being cut to length.

Type K soft copper tubing with a 0.5 in. (12.7 mm) outside diameter and a 0.049 in. (1.25 mm) wall thickness was used to protect the ends of the specimens in the grips.

2.4 Test Procedure

Fatigue tests on 69 specimens representing 6 different bar deformation patterns were conducted in air. The SMI4S60 specimens were protected in the grips using one piece of the multifold paper towel at each end and split copper tubing, while the other specimens were protected using split copper tubing only. The specimens were mounted, as shown in Fig. 2.10, in a servo-controlled hydraulic Instron machine, with a 110 kip (489 kN) loading capacity. The gripping pressure was 500 psi (3445 kPa) for No. 4 (13 mm) bars and 700 psi (4823 kPa) for No. 5 (16 mm) bars for all stress ranges. Sinusoidal loading was applied to the bars, varying from zero to a load based on the desired peak stress [20, 25, 30, or 35 ksi (138, 172, 207, and 241 MPa)]. The load was applied at a rate of 600 cycles per minute (10 Hz).

Bars in this study that sustained 2 million cycles without failure were considered to have been loaded below their fatigue strength. Tests on these specimens were stopped at 2 million cycles. When a specimen failed under cyclic load, the stroke of the load cell exceeded a preset maximum stroke value, causing the testing machine to stop automatically. Since the counter of the testing machine was not dependable, the number of cycles a bar sustained was obtained by a simple method, described next.

A battery operated clock and a piece of string were used in this method. The clock was tied to the upper load cell of the machine. The specimen was then mounted in the grips. One

end of the piece of string was tied to the bottom of the specimen; the other end was tied to a battery in the clock, making sure that the string was almost tight. The fatigue test was started in the load control mode, and the starting time was recorded. When the specimen broke, the lower grip moved down, causing the string to pull out the battery, stopping the clock. The number of cycles sustained was calculated based on the time difference and the loading frequency.

Tests in which fatigue failure occurred within the central portion of the bars were considered satisfactory. The results for any specimen that broke within the grips or shot peened portions were not used. Testing of each type of bar at a particular stress range was terminated when three satisfactory tests were obtained.

Because the fatigue test specimens were not perfectly straight and the grips of the machine may not have been perfectly aligned, tensile stress (detrimental to fatigue) may be introduced when a specimen was clamped in the jaws. To investigate the stresses introduced by the gripping system, the surface deformations of a No. 5 (16 mm) bar were removed in the central 4 in. (102 mm) portion of the specimen. The diameter of the section was 0.53 in. (13.5 mm), as shown in Table 2.4. Three strain gages were glued on the surface of the central part of the bar along the longitudinal axis. The gages were located 120 degrees apart around the bar perimeter. Copper tubing was used at both ends of the specimen. The load on the machine was preset at 0. Before the gripping pressure was applied, the initial strain readings of the three strain gages were recorded. Then the gripping pressure was applied and the machine was changed from Stroke Control to Load Control. Final strain values were then obtained. The process was repeated two more times as the specimen in the grips was repositioned. The results of the measurements are given in Table 2.4. The results indicate that the specimen was not in a zero stress state before the fatigue loading was applied, and that initial tensile stresses as high as 3 ksi (21 MPa) could have existed on the surface of the specimen during a test.

After testing of the Ch5S60, Ch5S, and N5S bars was completed, the Instron machine was recalibrated. According to the recalibration report, the nominal load was 95 percent of the actual load that the specimen sustained. Therefore, the actual stress ranges for these three types of bars were 21.05, 26.32, 31.58, and 36.84 ksi (145, 181, 218, and 254 MPa) instead of 20, 25, 30, and 35 ksi (138, 172, 207, and 241 MPa).

Using the specimen preparation and gripping method described in this Chapter, a success rate of greater than 80 percent was achieved for stress cycles from 0 ksi up to 35 ksi (241 MPa). Considering the pilot tests to establish the gripping techniques, about 150 specimens were tested. The following test results represent the 69 successful specimens.

2.5 Test Results

The experimental results and observations are summarized in this section. Detailed evaluation and discussion are presented in Chapter 3.

The fatigue test results are listed in Table 2.5. Plots of the S-N curves are shown in Fig. 2.11 for the No. 4 (13 mm) bars and in Fig. 2.12 for the No. 5 (16 mm) bars, respectively. The best fit curves for the bars were based on the average number of cycles at each stress range. Based on the report of Jhamb and MacGregor (1974a), the best fit equation was chosen in the logarithm form for each series:

$$\text{Log } N = A + B\,S$$

where Log N = logarithm of number of cycles, to the base 10; N (million)

S = stress range, ksi

A, B = coefficients

Fatigue crack sections for Ch4S60, SMI4S60, Ch5S60, Ch5S, N5S, and FK5S60 bars are shown in Figs. 2.13-2.18. The images were obtained with a scanner.

To investigate the effect of the surface geometry on fatigue behavior, samples of the bars were examined using a scanning electron microscope (SEM) interfaced with a digital image acquisition system. One sample was taken from each type of bar. The sample was cut through the longitudinal axis and prepared so that two complete deformations were left on both sides of the sample as shown in Table 2.6. The sample was cleaned using degreaser and 100 percent alcohol to remove surface dust. Before measuring the bar samples, the SEM was calibrated using a low magnification calibration standard with a 1 mm length and a 0.01 mm least reading. The SEM was calibrated in both the horizontal and vertical directions. Lug measurements were taken using the SEM images. Typical images are shown in Figs. 2.19-2.24.

Lug base radii, flank angles, and heights and widths were measured following the method described by Helgason et al. (1976). The lug base radii were determined using different diameter circles on a template. Flank angles were determined by drawing the lug base line and using a protractor to establish the angle that best represented the slopes of the sides of the lug. The lug height was determined as the greatest height from the lug base line. The lug width was determined as the distance along the lug base line between the points of intersection of the tangent lines used to determine the flank angles. A schematic illustration and the measurement results are shown in Table 2.6. The specimen has two lugs on each side, representing 2 of about 40 lugs between the bar identification marks. The results in Table 2.6 indicate that different sides (side 1 and side 2) of the specimen have different surface geometry. On the same side of the specimen, different lugs have different properties. Even for the same lug, the lug base radius (r_a, r_b) and flank angles (α, β) at the left and right side are different.

The following test results were observed.

Stress Range: As expected, fatigue strength decreased as the stress range increased. The Ch4S60 bars and SMI4S60 bars sustained 2 million cycles without breaking under stress ranges of 25 ksi and 20 ksi (172 and 138 MPa), respectively.

Bar Size: For a given stress range, the No. 4 (13 mm) bars exhibited a longer fatigue life than that the No. 5 (16mm) bars.

Surface Treatment: The Thermex bar (FK5S60) did not show superior fatigue behavior compared to the hot rolled bars of the same diameter (Ch5S60, Ch5S, and N5S).

Relative Rib Area: Of the No. 4 (13 mm) bars, the Ch4S60 bars had a higher value of R_r (0.128) and a longer fatigue life than the SMI4S60 bars (R_r = 0.064). For the No. 5 (16 mm) bars, the S-N curves show very little difference, especially between the Ch5S60, Ch5S, and N5S bars, with relative rib areas of 0.146, 0.100, and 0.076, respectively. The fatigue strength of the test bars was insensitive to relative rib area.

Fatigue Fractures: Examination of the fatigue fracture surfaces (Figs. 2.13-2.18) reveal that the fatigue cracks initiated at the root of a lug or at the intersection between a lug and a longitudinal rib. Fracture sections were normal to the bar axis or parallel to the lugs. Fatigue cracks started from both a single source or from multiple sources. For single source initiation, whenever a fatigue crack started, it propagated radially to the center of the bar along one plane, where the final fatigue fracture occurred (see the single source initiation cases in Figs. 2.13-2.18). For multiple source initiation, the fatigue cracks either propagated radially to the center of the bar along one plane, where the final fracture surface occurred (see the multiple source initiation cases in Figs. 2.13, 2.14, and 2.18) or propagated individually along different planes (see the multiple source initiation cases in Fig. 2.15, 2.16, and 2.17) radially to the center of the bar, where the crack planes gradually merged into a single plane, which served as the final fracture surface.

For the SMI4S60 bars, Ch5S60 bars, Ch5S bars, and N5S bars, the fatigue crack zone is a smooth and dull-appearing region, surrounded by a rough and light-appearing crystalline tension failure zone. The boundary between the fatigue zone and the tension failure zone was very clear (Figs. 2.14-2.17). For the Ch4S60 and FK5S60 bars, the fatigue crack zone was also smooth and dull-appearing, surrounded by a rough tension failure zone. However, the

tension failure zone did have a crystalline appearance and the boundary between the two zones was not clear (Fig. 2.13 and Fig. 2.18).

Surface Geometry: Based on the images shown in Figs. 2.19-2.24 and the measurements in Table 2.6, it is clear that different deformation patterns have completely different lug geometries. For the No. 4 (13 mm) bars, the Ch4S60 and SMI4S60 bars have critical r/h values of 1.31 and 0.79, respectively. For the No. 5 (16 mm) bars, the Ch5S60, Ch5S, and N5S bars have slightly different critical r/h values of 0.78, 0.80, and 0.90, respectively. While the FK5S60 bars have the lowest critical r/h value, 0.45, in the tests.

CHAPTER THREE

EVALUATION AND DISCUSSION OF TEST RESULTS

3.1 General

In this chapter, the results reported in Chapter 2 are evaluated. The effects of bar diameter, surface geometry, and relative rib area on the fatigue performance of the bars are discussed. The fatigue strength of reinforcing bars tested in this study is compared with previous tests on bars in air and with the design criterion given by the AASHTO Bridge Specifications (1996).

3.2 Effect of Bar Diameter

In the current tests, the fatigue behavior of the No. 4 (13 mm) bars is superior to that of the No. 5 (16 mm) bars. The effect of bar diameter on the fatigue behavior of bars is shown in Fig. 3.1. This observation is in agreement with results reported by McDermott (1965, 1971), MacGregor, Jhamb, and Nuttall (1971), Helgason et al. (1976), and Moss (1980) that showed that the fatigue strength of deformed reinforcing bar decreases as the bar diameter increases.

The increase in fatigue strength with decreased bar diameter, as explained by Weisman (1969), results from the additional work needed to produce smaller size bars. The additional work in the rolling operation results in a finer grain structure and the fragmentation and dispersion of inclusions. These factors produce an increase in fatigue strength. Osgood (1970) also attributes a significant part of the size effect to the total amount of work that the material receives, particularly the reduction in thickness from the original ingot to the final form. Kravshenko (1964) points out that an increase in the absolute dimensions of a bar results in an increase in the surface area that is subjected to maximum stress. Thus, the larger surface area increases the likelihood of a fatigue crack being initiated. Tetelman and McEvily

(1967) support Kravshenko's opinion and state that there is a size effect related to the probability of finding a critical flaw within the most highly stressed regions. ACI Committee 215 (1974) attributes the size effect to the probability of finding a critical notch on the bar surface, supporting the opinion of Tetelman and McEvily (1967). Both the extra work on the smaller bars and the increased surface area on the larger bars likely play a role in the effect of bar size on fatigue strength.

3.3 Effect of Surface Geometry

The transverse deformations on the surface of reinforcing bars provide improved bond characteristics between the concrete and the steel. The surface geometry or deformation pattern is designed primarily for bond characteristics, not fatigue considerations. The transverse deformations, in addition to transmitting forces between steel and concrete, also cause stress concentrations on the surface of the bar, which serve as potential fatigue crack initiators. In the current tests, fatigue cracks started at the root of a lug or at the intersection between a longitudinal rib and a lug, where the highest stress concentrations exist. The effect of manufacture's identification marks on the fatigue behavior of the bars was not considered in this study.

As described in Chapter 1, stress concentrations are related to the lug base radius-to-height ratio (r/h), to the lug width-to-height ratio (w/h), and to the flank angles. The lug base radius-to-height ratio (r/h) is considered to be the prime factor affecting the stress concentration factors (Hanson, Burton, and Hognestad 1968, MacGregor, Jhamb, and Nuttall 1971, Jhamb and MacGregor 1974a, 1974b, Helgason et al. 1976, Zheng and Abel 1998, 1999).

Based on the fatigue results shown in Table 2.5 and the SEM measurements shown in Table 2.6, the effect of surface geometry such as the critical r/h ratio, average w/h ratio, and the sharpest average flank angles are shown in Figs. 3.2-3.4. Comparisons are made based on the average number of cycles (from best-fit lines) at 25 and 35 ksi (172 and 241 MPa) for

each pattern. In Fig. 3.4, for each type of bar, the sharpest average flank angle was obtained by comparing the values of the average left flank angles and the average right flank angles of the two lugs on each side of the specimen, as shown in Table 2.6.

For the No. 4 (13 mm) bars, N increases as the critical r/h ratio increases (Fig. 3.2). N decreases as the average w/h ratio increases (Fig. 3.3). Thus, increased r/h ratio and decreased w/h ratio result in increased fatigue strength. This is in agreement with the conclusions of Zheng and Abel (1998). However, as shown in Fig. 3.4, N increases as the sharpest average flank angle increases.

For the No. 5 (16 mm) bars, N increases as the critical r/h ratio increases (Fig. 3.2), also in agreement with Zheng and Abel's (1998) conclusions. However, the effects of average w/h ratio and flank angle on the fatigue performance of the bars are not clear (Figs. 3.3 and 3.4).

The current results confirm the previous conclusions that the r/h value has a significant influence on the fatigue behavior of deformed bars. The w/h value and flank angles have much less effect. The lower the r/h ratio, the higher the resulting stress concentration. Increasing the r/h value decreases the stress concentration, and, thus, results in an increase in fatigue strength.

As mentioned in Chapter 1, Jhamb and MacGregor (1974b) reported that the fatigue strength of deformed bars decreases when the r/h ratio is less than 1.25 and is almost constant for r/h ratios greater than 1.25. In the current study, only the Ch4S60 bars had a critical r/h ratio (1.31) greater than 1.25. Therefore, determining of fatigue strength is almost constant for r/h ratios greater than 1.25 is not possible. However, for critical r/h ratios less than 1.25, the number of cycles sustained clearly decreases as the r/h ratio decreases.

3.4 Effect of Relative Rib Area

As described in Chapter 1, high relative rib area bars have advantages over conventional

bars. But until the current study, the effect of increased relative rib area on the fatigue behavior of deformed reinforcing bars has been unclear.

In this section, the effect of relative rib area, R_r, on the fatigue behavior of deformed bars will be discussed using both the test results and the expression that defines R_r. First, the effect of R_r values on the fatigue performance of bars in this study is shown in Fig. 3.5. As shown in the figure, an increase in the relative rib area of the bars tested in this study did not result in a decrease in the fatigue life of the bars. Specifically, for the No. 4 (13 mm) bars, N increases as R_r increases. The fatigue strength of the Ch4S60 bars (R_r = 0.128) is superior to that of SMI4S60 bars (R_r = 0.064). For the No. 5 (16mm) bars, the Ch5S60 (R_r = 0.146) and Ch5S (R_r = 0.100) bars are high relative rib area bars, while the N5S (R_r = 0.076) and FK5S60 (R_r = 0.088) bars are conventional bars. The high relative rib area bars did not show lower fatigue strength than the same diameter conventional bars. The fatigue performance of deformed reinforcing bars, thus, appears to be insensitive to relative rib area.

The relative rib area, R_r, is defined as the ratio of projected rib area normal to the bar axis to the product of the nominal bar diameter and the average center-to-center rib spacing. It can be calculated using Eq. (2.1).

$$R_r = \frac{h_r}{s_r}\left(1 - \frac{\sum gaps}{p}\right) \qquad (2.1)$$

In the equation, there are four variables used to determine the value of R_r. Only the variable, p, has a direct relation to the fatigue behavior of the bars because the bar perimeter is proportional to the bar diameter. No evidence shows that the other variables, average rib height (h_r), average deformation spacing (s_r), and sum of gaps ($\sum gaps$), influence the fatigue performance of reinforcing bars. For bars with the same diameter but with different values of R_r, the bar perimeter is a constant, and R_r is totally determined by the other three variables,

h_r, s_r, and Σgaps. Because none of these has any effect on fatigue strength, R_r should have no effect on the fatigue strength of reinforcing bars.

The results clearly demonstrate that high relative rib area bars, because of the value of R_r alone, should not be expected to show lowered fatigue strength compared with conventional bars of the same diameter.

3.5 Comparison with Previous Test Results in Air

In the current study, fatigue tests were conducted on No. 4 (13 mm) and No. 5 (16 mm) deformed bars. In this section, fatigue test results of small diameter deformed bars in air from previous studies are compared with the current results.

In McDermott's 1965 report, the fatigue tests were conducted in air with a stress ratio between 0 and ± 0.03. The DI-LOK No. 4 (13 mm) bars had a fatigue strength of 39 ksi (269 MPa) at 3 million cycles.

In McDermott's 1971 report, No. 4 (13 mm) helix bars were tested in air with a stress ratio of 0. The test results showed that the fatigue strength of the No. 4 (13 mm) bars was 37.5 ksi (258 MPa) at 4 million cycles.

In Moss's 1980 report, fatigue tests on British high-yield bars were conducted in air. The fatigue strength of the 16 mm diameter continuous bars under constant amplitude cyclic loading (stress ratio = 0.2) was 190 MPa (28 ksi) at 10^8 cycles.

In Matsumoto's 1988 report, Grade 60 No. 3 (9.53 mm) bars were tested in air with a minimum stress of 6 ksi (41 MPa). The fatigue strength of the bars was 32 ksi (221 MPa) at 2 million cycles.

In Zheng and Abel's 1999 report, the fatigue characteristics of Australian-made Tempcore 12 mm (No. 4) to 36 mm (No. 11) bars were tested in air with a stress ratio of 0. The fatigue strengths of the 12 mm (No. 4) and the 16 mm (No. 5) bars were 270 and 310 MPa (39 and 45 ksi), respectively, corresponding to 5 million cycles.

In the current study, fatigue tests of No. 4 (13 mm) and No. 5 (16 mm) bars were conducted in air at a stress ratio of 0. The fatigue strengths of the Ch4S60 and SMI4S60 bars were 25 ksi and 20 ksi (172 and 138 MPa), corresponding to 2 million cycles, respectively. However, all of the No. 5 (16 mm) bars failed in less than 1 million cycles at 21.05 ksi (145 MPa) [20 ksi (138 MPa) for FK5S60 bars]. Thus, the fatigue performance of the bars tested in this study was inferior to that obtained in the previous tests. One reason may come from the fact, as described in Chapter 2 (Table 2.4), that before the fatigue load was applied, tensile stresses were induced in the specimens when the specimens were gripped. These tensile stresses [as high as 3 ksi (21 MPa)] result in an increased minimum stress, a positive stress ratio instead of 0, and a higher maximum stress level. All of these factors are known to decrease fatigue strength.

3.6 Comparison with AASHTO Fatigue Design Criteria

In real reinforced concrete members, it is hard to know the exact state of stress at the root of a rolled deformation. It is also hard to know how forces are transmitted between reinforcing bars and concrete at crack locations in the concrete. No statistically valid comparison between fatigue tests of reinforcing bars in air and embedded in concrete has been carried out (ACI Committee 215 1974). Questions exist as to whether a bar has the same fatigue strength when tested in air as it does in a concrete member. And so far, no test has been standardized in the United States to determine the fatigue properties of deformed reinforcing bars. Based on the equations developed by Helgason et al. (1976), the AASHTO Bridge Specifications (1996) provides a simplified design criterion for straight deformed hot rolled reinforcing bars embedded in concrete. According to that criterion, the design stress range is

$$f_f = 21 - 0.33f_{min} + 8(r/h) \text{ ksi} \qquad (3.1a)$$

$$f_f = 145 - 0.33f_{min} + 55(r/h) \text{ MPa} \qquad (3.1b)$$

where f_f = stress range, in ksi (MPa)

f_{min} = algebraic minimum stress, tension positive, compression negative, in ksi (MPa)

r/h = ratio of base radius to rib height, a value of 0.3 can be used

In the current tests, the minimum stress is 0 ksi. According to Eq. (3.1) above, the design stress range should be 23.4 ksi (161.5 MPa). This means that for any stress range below 23.4 ksi (161.5 MPa), a bar in this experiment should sustain virtually an unlimited number of cycles without breaking. Only the fatigue behavior of the Ch4S60 bars met this criterion. Corresponding to 2 million cycles, the Ch4S60 bars did not break at a stress range of 25 ksi (172 MPa). The SMI4S60 bars did not break at a stress range of 20 ksi (138 MPa) and were not evaluated at f_f = 23.4 ksi.

The No. 5 (16 mm) bars in this study deviated significantly from the criteria in Eq. (3.1). The bars broke after less than 1 million cycles for a stress range of 21.05 ksi (145 MPa) [20 ksi (138 MPa) for FK5S60 bars]. These results, however, do not mean that the No. 5 (16 mm) bars in this study are not qualified for use in concrete structures subjected to fatigue loading.

The principle reasons are two fold, both due to the severity of the current tests. First, the bars had added stresses, as high as 3 ksi (21 MPa), induced due to the gripping mechanism. Second, testing in air results in a shorter fatigue life than testing in concrete where the tensile strength of concrete between cracks helps to limit the effect of the cyclic loading on reinforcing steel. Thus, for most of the length of reinforcing bars embedded in concrete, the tension stress is well below the value calculated by neglecting the tensile strength of the concrete. Only at flexural cracks will reinforcing steel be subjected to the full stress, and statistically, those locations are not expected to expose a region of the bar with the lowest fatigue life. This contrasts with tests in air that involve a length of bar, all of which is

exposed to the maximum tensile stress, allowing the region with the lowest fatigue life to govern.

CHAPTER FOUR

SUMMARY AND CONCLUSIONS

4.1 Summary

The purpose of this research is to study the fatigue performance of high relative rib area bars and compare their performance with conventional bars. This study includes a review of previous work; results from fatigue tests on 69 specimens under axial loading in air; and a discussion of the factors that may influence the fatigue behavior of the bars. The major test variables in this research are the stress range [20, 25, 30, and 35 ksi (138, 172, 207, and 241 MPa)] with 0 ksi minimum stress, bar diameter [No. 4 (13mm) and No. 5 (16mm)], surface geometry (6 different bar deformation patterns), and relative rib area (0.064 to 0.146).

4.2 Conclusions

The following conclusions are made based on the test results and the discussion presented in this report:

1. The results confirm previous conclusions that the stress range is the predominant factor influencing the fatigue strength of reinforcing bars.
2. The results tend to confirm previous conclusions that there exists a stress range, the fatigue strength above which a bar is certain to break in fatigue and below which a bar can sustain a virtually unlimited number of cycles without fatigue failure.
3. Bar diameter has a significant effect on the fatigue strength of reinforcing bars. For bars subjected to the same stress range, an increase in bar diameter results in a decrease in fatigue strength.
4. Surface geometry has a great effect on the fatigue strength of reinforcing bars. The lug base radius-to-height ratio (r/h) was found to have a primary influence on the

fatigue strength of the bars. For bars with the same diameter, the lower the r/h ratio, the lower the fatigue strength.

5. Relative rib area value, R_r, does not effect the fatigue strength of deformed reinforcing bars. High relative rib area bars exhibit similar fatigue performance to conventional bars of the same bar diameter, subjected to the same stress range.

REFERENCES

AASHTO. 1996. "*Standard Specifications for Highway Bridges,*" American Association of State Highway and Transportation Officials, Washington, D.C., pp. 183-184.

ACI Committee 215. 1974. *Consideration for Design of Concrete Structures Subjected to Fatigue Loading (ACI 215R-74, 1997, Revised 1992),* American Concrete Institute, Farmington Hills, MI, 24 pp.

ACI Innovation Task Group 2. 1998. *Splice and Development Length of High Relative Rib Area Reinforcing Bars (ACI 2.1-98), An ACI Provisional Standard,* American Concrete Institute, Farmington Hills, MI.

ASTM. "Standard Specification for Deformed and Plain Billet-Steel Bars for Concrete Reinforcement. (ASTM A 615/A 615M-96a)," *1999 Annual Book of ASTM Standards,* Vol. 1.04, American Society of Testing and Materials, Philadelphia, PA, pp. 308-312.

ASTM. "Standard Specification for Rail-Steel Deformed and Plain Bars for Concrete Reinforcement. (ASTM A 616/A 616M-96a)," *1999 Annual Book of ASTM Standards,* Vol. 1.04, American Society of Testing and Materials, Philadelphia, PA, pp. 313-316.

ASTM. "Standard Specification for Axle-Steel Deformed and Plain Bars for Concrete Reinforcement. (ASTM A 617/A617M-96a)," *1999 Annual Book of ASTM Standards,* Vol. 1.04, American Society of Testing and Materials, Philadelphia, PA, pp. 317-320.

ASTM. "Standard Specification for Low-Alloy Steel Deformed and Plain Bars for Concrete Reinforcement. (ASTM 706/706M-96b)," *1999 Annual Book of ASTM Standards,* Vol. 1.04, American Society of Testing and Materials, Philadelphia, PA, pp. 346-350.

Burton, K. T. 1965. "Fatigue Tests of Reinforcing Bars," *Journal,* PCA Research and Development Laboratories, Vol. 7, No. 3, Sept., pp. 13-23. Also, *Development Department Bulletin* No. D93, Portland Cement Association.

Clark, A. P. (1946) "Comparative Bond Efficiency of Deformed Concrete Reinforcing Bars," ACI Journal, *Proceedings* Vol. 43, No. 4, Dec., pp. 381-400.

Darwin, D. and Graham, E. K. 1993a. "Effect of Deformation Height and Spacing on Bond Strength of Reinforcing Bars," *SL Report* 93-1, University of Kansas Center for Research, Lawrence, Kansas, Jan., 68 pp.

Darwin, D. and Graham, E. K. 1993b. "Effect of Deformation Height and Spacing on Bond Strength of Reinforcing Bars," *ACI Structural Journal,* Nov.-Dec., Vol. 90, No. 6, pp. 646-657.

Darwin, D.; Tholen, M. L.; Idun, E. K.; and Zuo, J. 1995. "Splice Strength of High Relative Rib Area Reinforcing Bars," *SL Report* 95-3, University of Kansas Center for Research, Lawrence, Kansas, May, 58 pp.

Darwin, D.; Tholen, M. L.; Idun, E. K.; and Zuo, J. 1996. "Splice Strength of High Relative Rib Area Reinforcing Bars," *ACI Structural Journal*, Vol. 93, No. 1, Jan-Feb, pp. 95-107.

Hanson, J. M.; Burton, K. T.; and Hognestad, E. 1968. "Fatigue Tests of Reinforcing Bars – Effect of Deformation Pattern," *Journal*, PCA Research and Development Laboratories, Vol. 10, No. 3, Sept., pp. 2-13. Also, *Development Department Bulletin* No. D145, Portland Cement Association.

Hanson, J. M.; Helgason, Th.; and Ball, C. 1972. "Fatigue Strength of Experimental No. 8 Grade 60 Helix Reinforcing Bars," Research and Development Laboratories, Cement and Concrete Research Institute, Portland Cement Association, June, 29 pp.

Helgason, T.; Hanson, T. M.; Somes, N. F.; Corley, W. G.; and Hognestad, E. 1976. "Fatigue Strength of High Yield Reinforcing Bars," *National Cooperative Highway Research Program* Report 164, Transportation Research Board, National Research Council, Washington, D. C.

Jhamb, I.C. and MacGregor, J. G. 1974a. "Effect of Surface Characteristics On Fatigue Strength of Reinforcing Steel," *Abeles Symposium on Fatigue of Concrete*, ACI SP 41, American Concrete Institute, Detroit, pp. 139-150.

Jhamb, I.C. and MacGregor, J. G. 1974b. "Stress Concentrations Caused By Reinforcing Bar Deformations," *Abeles Symposium on Fatigue of Concrete*, ACI SP 41, American Concrete Institute, Detroit, pp. 169-182.

Kravshenko, P. Ye. 1964. *Fatigue Resistance*, Pergamon Press, New York, 112 pp.

MacGregor, J. G.; Jhamb, I. C.; and Nuttall, N. 1971. "Fatigue Strength of Hot-Rolled Reinforcing Bars," ACI Journal, *Proceedings* Vol. 68, No. 3, Mar., pp. 169-179.

Matsumoto, N. 1988. "A Study on Fatigue Behavior of Cold-Worked Deformed Reinforcing Bars," *Proceedings of Japan Society of Civil Engineers*, Vol. 9, No. 396, Aug., pp. 177-186.

McDermott, J. F. 1965. "Fatigue Tests of A 432 High-Strength-Steel Reinforcing Bars," Applied Research Laboratory Report 57.019-901 (5), November 12, 23 pp.

McDermott, J. F. 1969. "Fatigue Characteristics of Reinforcing Bars With Various Deformation Patterns," Applied Research Laboratory Report 45.019-001 (1), July 3, 30 pp.

McDermott, J. F. 1971. "Fatigue Strength of Grade 60 Reinforcing Bars With A Spiral Deformation Pattern," Applied Research Laboratory Report 57.019-452 (5), March 26, 20 pp.

Moss, D. S. 1980. "Axial Fatigue of High-Yield Reinforcing Bars In Air," Transport and Road Research Laboratory, Department of The Environment, Department of Transport, *Supplementary Report* 622.

Narayanaswamy, V. P.; Gupta, V. K.; Chhauda, J. N.; and Rajaraman, A. 1977. "Experimental Investigation on The Fatigue Behavior of Cold-Worked Deformed Bars," *Materials and Structures*, Vol. 10, No. 57, May-June, pp. 153-158.

Osgood, C. 1970. *Fatigue Design*, Wiley-Interscience, New York.

Pfister, J. F. and Hognestad, E. 1964. "High Strength Bars as Concrete Reinforcement, Part 6, Fatigue Tests," *Journal*, PCA Research and Development Laboratories, Vol. 6, No. 1, Jan., pp. 65-84. Also, *Development Department Bulletin* No. D74, Portland Cement Association.

Tetelman, A. S. and McEvily, Jr., A. J. 1967. *Fracture of Structural Materials*, Wiley, New York, 697 pp.

Thandavamoorthy, T. S. 1999. "Static And Fatigue of High-Ductility Bars Reinforced Concrete Beams," *Journal of Materials in Civil Engineering*, ASCE, Feb., pp. 41-50.

Weisman, M. H. 1969 "Detailed Design and Manufacturing Considerations," *Metal Fatigue; Theory and Design*, ed. A. F. Madayag, Wiley, New York.

Zheng, H. and Abel, A. 1998. "Stress Concentration and Fatigue of Profiled Reinforcing Steels," *International Journal of Fatigue*, Vol. 20, No. 10, Nov., pp. 767-773.

Zheng, H. and Abel, A. 1999. "Fatigue Properties of Reinforcing Steel Produced By TEMPCORE Process," *Journal of Materials in Civil Engineering*, ASCE, Vol. 11, No. 2 May, pp. 158-165.

Table 2.1

Deformation Properties of Reinforcing Bars

Bar Identification	Nominal Diameter (in.)	Weight (lb/ft)	% Light or Heavy	Rib Angle + (degrees)	Avg. Rib Spacing (in.)	Rib Height* ASTM (in.)	Rib Height* Avg.** (in.)	Average ∑gaps (in.)	Relative Rib Area***
Ch4S60	0.500	0.638	4.5% L	65	0.206	0.035	0.034	0.338	0.128
SMI4S60	0.500	0.639	4.3% L	90	0.333	0.028	0.027	0.326	0.064
Ch5S60	0.625	1.017	2.5% L	65	0.258	0.047	0.047	0.398	0.146
Ch5S	0.625	1.032	1.1% L	70	0.275	0.039	0.036	0.413	0.100
N5S	0.625	1.011	3.1% L	70	0.350	0.037	0.034	0.359	0.076
FK5S60	0.625	1.018	2.4% L	90	0.409	0.044	0.043	0.335	0.088

+ Angle of transverse rib to the bar axis

* See Table 2.2 for detailed rib height measurement

** Average rib height (see section 2.2)

*** See Fig. 2.2 and Eq. 2.1

1 in. = 25.4 mm; 1 lb/ft = 1.49 kg/m;

Table 2.2

Rib Heights of Transverse Deformations on Bars Investigated

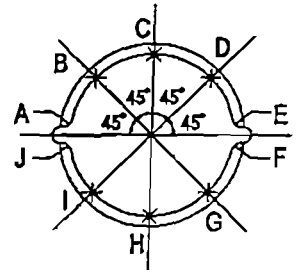

Bar Identification	Rib Heights * (mm)									
	A	B	C	D	E	F	G	H	I	J
Ch4S60	0.68	0.90	0.87	1.00	0.86	0.74	0.86	0.86	0.85	0.72
	0.68	0.93	0.85	0.98	0.88	0.72	0.83	0.87	0.83	0.72
	0.70	0.93	0.85	0.95	0.85	0.73	0.85	0.87	0.84	0.74
	0.70	0.95	0.86	0.98	0.88	0.71	0.84	0.87	0.85	0.73
	0.68	0.94	0.86	0.99	0.87	0.73	0.80	0.86	0.85	0.72
SMI4S60	0.61	0.72	0.67	0.73	0.74	0.62	0.73	0.69	0.65	0.56
	0.61	0.72	0.66	0.73	0.74	0.62	0.75	0.70	0.65	0.55
	0.63	0.73	0.66	0.74	0.75	0.62	0.75	0.70	0.64	0.54
	0.63	0.73	0.67	0.73	0.74	0.63	0.74	0.69	0.62	0.54
	0.63	0.73	0.66	0.73	0.74	0.62	0.74	0.70	0.63	0.55
Ch5S60	1.42	1.32	1.25	1.25	1.15	1.00	1.32	0.82	1.25	1.15
	1.45	1.33	1.23	1.26	1.13	1.00	1.33	0.85	1.25	1.14
	1.41	1.32	1.20	1.26	1.10	1.00	1.34	0.95	1.25	1.11
	1.43	1.31	1.23	1.25	1.10	1.03	1.34	0.85	1.25	1.14
	1.43	1.32	1.22	1.25	1.09	1.00	1.33	0.83	1.26	1.14

Table 2.2 (continued)

Rib Heights of Transverse Deformations on Bars Investigated

Bar Identification	Rib Heights * (mm)									
	A	B	C	D	E	F	G	H	I	J
Ch5S	0.60	0.96	0.86	1.04	0.89	1.02	1.26	0.88	0.90	0.56
	0.61	0.98	0.89	1.03	0.86	1.02	1.22	0.87	0.92	0.56
	0.57	0.99	0.90	1.03	0.84	1.07	1.21	0.88	0.91	0.54
	0.63	0.96	0.89	1.00	0.82	1.10	1.24	0.86	0.89	0.55
	0.61	0.95	0.88	1.01	0.85	1.16	1.20	0.88	0.92	0.52
N5S	0.66	0.77	0.95	1.20	0.80	0.56	0.70	0.90	0.97	0.64
	0.64	0.79	0.99	1.17	0.80	0.57	0.70	0.93	0.96	0.69
	0.63	0.83	0.99	1.14	0.85	0.55	0.69	0.95	0.99	0.66
	0.62	0.85	0.97	1.17	0.83	0.56	0.67	0.94	1.01	0.64
	0.60	0.82	0.95	1.13	0.80	0.55	0.72	0.95	0.99	0.62
FK5S60	1.14	1.15	1.04	1.17	1.13	1.06	0.99	1.05	1.17	1.08
	1.15	1.15	1.03	1.22	1.14	1.04	1.00	1.06	1.20	1.13
	1.13	1.18	1.04	1.19	1.13	1.04	1.00	1.06	1.22	1.12
	1.12	1.17	1.05	1.17	1.13	1.07	0.99	1.06	1.19	1.15
	1.12	1.17	1.04	1.17	1.08	1.05	1.01	1.06	1.21	1.13

* Measured using Starrett dial gage with 0.01 mm least reading

Table 2.3

Mechanical Properties of Reinforcing Bars

Bar Name	Diameter (in)	L (in)	L' (in)	ΔL (in)	Elongation ΔL/L (%)	Yield Strength (ksi)	Tensile strength (ksi)
Ch4S60	0.500	8.000	9.500	1.500	18.75	71.0	103.9
	0.500	8.000	9.250	1.250	15.63	75.8	108.4
	0.500	8.000	9.250	1.250	15.63	74.7	107.6
SMI4S60	0.500	8.000	9.250	1.250	15.63	63.2	107.4
	0.500	8.000	9.375	1.375	17.19	66.8	110.0
	0.500	8.000	9.375	1.375	17.19	64.7	107.9
Ch5S60	0.625	8.000	9.500	1.500	18.75	69.5	106.1
	0.625	8.000	9.300	1.300	16.25	71.6	102.9
	0.625	8.000	9.350	1.350	16.88	71.1	102.3
Ch5S	0.625	8.000	9.500	1.500	18.75	65.3	102.7
	0.625	8.000	9.500	1.500	18.75	66.3	99.6
	0.625	8.000	9.450	1.450	18.13	65.8	98.9
N5S	0.625	8.000	9.450	1.450	18.13	71.1	115.3
	0.625	8.000	9.400	1.400	17.50	72.6	109.8
	0.625	8.000	9.450	1.450	18.13	72.1	109.5
FK5S60	0.625	8.000	9.525	1.525	19.06	77.4	103.4
	0.625	8.000	9.375	1.375	17.19	78.9	103.4
	0.625	8.000	9.500	1.500	18.75	81.2	103.2

where: L = original gage length, in.

L' = final gage length, in.

ΔL = elongation of the bar, in.

1 in. = 25.4 mm; 1 ksi = 6.89 MPa;

Table 2.4
Stresses Introduced by Gripping System

Measuring Time	Strain Gage Number	Strain (microstrain)	Stress (ksi)
1st Time	1	-14	-0.41
	2	41	1.19
	3	31	0.90
2nd Time	1	-12	-0.35
	2	34	0.99
	3	92	2.67
3rd Time	1	-50	-1.45
	2	37	1.07
	3	53	1.54

+ strain reading before the gripping pressure was applied

* strain reading after the gripping pressure was applied

modulus of elasticity of the steel bar = 29 x 10^3 ksi

1 ksi = 6.89 MPa

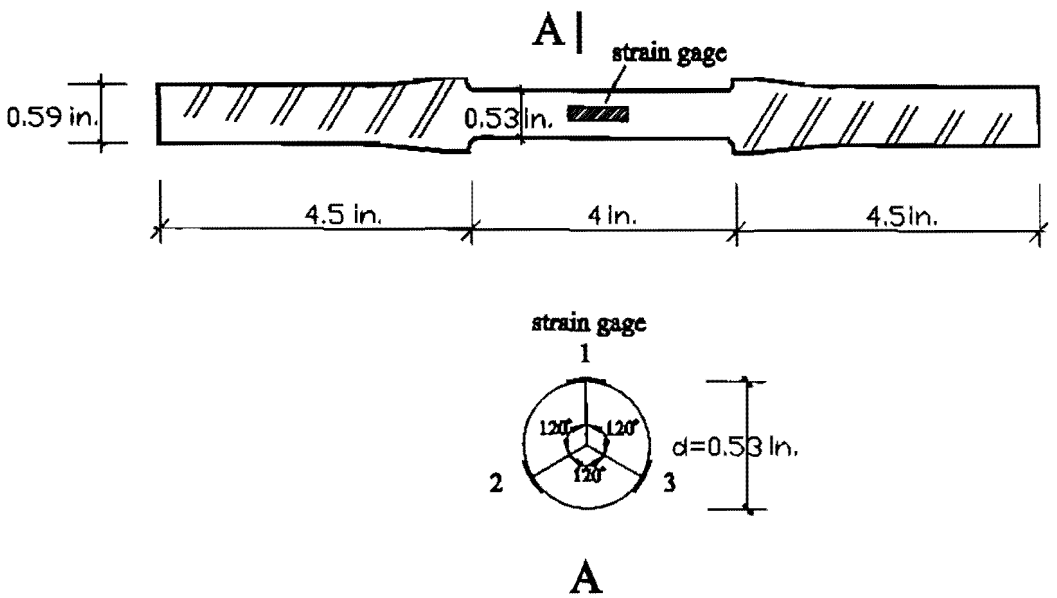

Table 2.5
Fatigue Test Results of Reinforcing Bars

Ch4S60 bars:

Stress Range	Number of Cycles	Crack Initiation Location	Fracture Section
35 ksi	623,800	root of a lug	angled to the bar axis (parallel to lug direction)
	823,800	root of a lug	angled to the bar axis (parallel to lug direction)
	706,500	intersection between a lug and a longitudinal rib	angled to the bar axis (parallel to lug direction)
30 ksi	1,211,300	intersection between a lug and a longitudinal rib	angled to the bar axis (parallel to lug direction)
	912,000	root of a lug	angled to the bar axis (parallel to lug direction)
	1,295,900	intersection between a lug and a longitudinal rib	angled to the bar axis (parallel to lug direction)
25 ksi	2,000,000*	N/A	N/A
	2,000,000*	N/A	N/A
	2,000,000*	N/A	N/A

*** bar did not break**

SMI4S60 bars:

Stress Range	Number of Cycles	Crack Initiation Location	Fracture Section
35 ksi	601,400	root of a lug	normal to the bar axis
	460,600	root of a lug	normal to the bar axis
	688,500	root of a lug	normal to the bar axis
30 ksi	933,700	root of a lug	normal to the bar axis
	801,900	root of a lug	normal to the bar axis
	868,900	root of a lug	normal to the bar axis
25 ksi	1,528,400	root of a lug	normal to the bar axis
	1,144,000	root of a lug	normal to the bar axis
	1,373,700	root of a lug	normal to the bar axis
20 ksi	2,000,000*	N/A	N/A
	2,000,000*	N/A	N/A
	2,000,000*	N/A	N/A

*** bar did not break**

1 ksi = 6.89 MPa

Table 2.5 (continued)
Fatigue Test Results of Reinforcing Bars

Ch5S60 bars:

Stress Range	Number of Cycles	Crack Initiation Location	Fracture Section
36.84 ksi	171,600	intersection between a lug and a longitudinal rib	normal to bar axis
	164,600	intersection between a lug and a longitudinal rib	normal to bar axis
	168,900	intersection between a lug and a longitudinal rib	normal to bar axis
31.58 ksi	243,300	intersection between a lug and a longitudinal rib	normal to bar axis
	317,200	intersection between a lug and a longitudinal rib	normal to bar axis
	266,600	intersection between a lug and a longitudinal rib	normal to bar axis
26.32 ksi	409,800	intersection between a lug and a longitudinal rib	normal to bar axis
	394,400	intersection between a lug and a longitudinal rib	normal to bar axis
	381,700	intersection between a lug and a longitudinal rib	normal to bar axis
21.05 ksi	643,600	intersection between a lug and a longitudinal rib	normal to bar axis
	676,600	intersection between a lug and a longitudinal rib	normal to bar axis
	651,100	intersection between a lug and a longitudinal rib	normal to bar axis

1 ksi = 6.89 MPa

Table 2.5 (continued)
Fatigue Test Results of Reinforcing Bars

Ch5S bars:

Stress Range	Number of Cycles	Crack Initiation Location	Fracture Section
36.84 ksi	204,100	intersection between a lug and a longitudinal rib	normal to bar axis
	169,900	intersection between a lug and a longitudinal rib	normal to bar axis
	193,500	intersection between a lug and a longitudinal rib	normal to bar axis
31.58 ksi	281,200	intersection between a lug and a longitudinal rib	normal to bar axis
	255,300	intersection between a lug and a longitudinal rib	normal to bar axis
	312,800	intersection between a lug and a longitudinal rib	normal to bar axis
26.32 ksi	430,800	intersection between a lug and a longitudinal rib	normal to bar axis
	417,800	intersection between a lug and a longitudinal rib	normal to bar axis
	424,400	intersection between a lug and a longitudinal rib	normal to bar axis
21.05 ksi	720,700	intersection between a lug and a longitudinal rib	normal to bar axis
	659,800	intersection between a lug and a longitudinal rib	normal to bar axis
	701,700	intersection between a lug and a longitudinal rib	normal to bar axis

1 ksi = 6.89 MPa

Table 2.5 (continued)
Fatigue Test Results of Reinforcing Bars

N5S bars:

Stress Range	Number of Cycles	Crack Initiation Location	Fracture Section
36.84 ksi	210,800	root of a lug	normal to the bar axis
	235,200	root of a lug	angled to the bar axis (parallel to lug direction)
	215,100	intersection between a lug and a longitudinal rib	normal to the bar axis
31.58 ksi	293,600	root of a lug	normal to the bar axis
	272,900	root of a lug	normal to the bar axis
	210,300	root of a lug	angled to the bar axis (parallel to lug direction)
26.32 ksi	410,400	root of a lug	angled to the bar axis (parallel to lug direction)
	396,600	root of a lug	angled to the bar axis (parallel to lug direction)
	436,600	root of a lug	normal to the bar axis
21.05 ksi	702,200	root of a lug	normal to the bar axis
	660,400	root of a lug	normal to the bar axis
	679,600	root of a lug	normal to the bar axis

FK5S60 bars:

Stress Range	Number of Cycles	Crack Initiation Location	Fracture Section
35 ksi	137,100	root of a lug	normal to the bar axis
	173,000	root of a lug	normal to the bar axis
	162,900	root of a lug	normal to the bar axis
30 ksi	270,100	root of a lug	normal to the bar axis
	246,300	root of a lug	normal to the bar axis
	222,000	root of a lug	normal to the bar axis
25 ksi	360,600	root of a lug	normal to the bar axis
	374,200	root of a lug	normal to the bar axis
	282,000	root of a lug	normal to the bar axis
20 ksi	657,400	root of a lug	normal to the bar axis
	566,900	root of a lug	normal to the bar axis
	604,100	root of a lug	normal to the bar axis

1 ksi = 6.89 MPa

Table 2.6

Measurements of Lug Properties Obtained with Scanning Electron Microscope

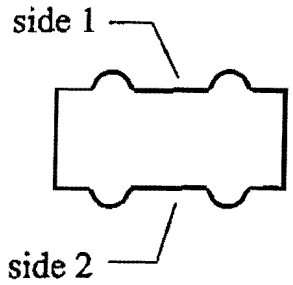

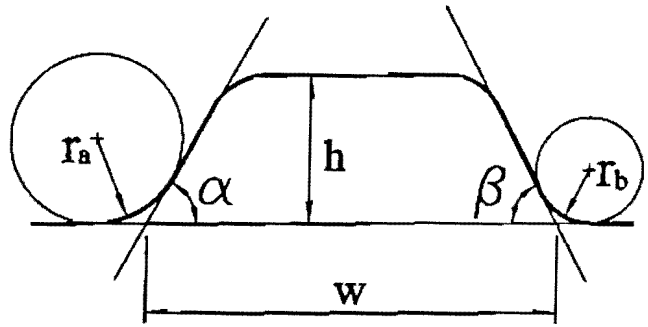

Bar Identification		α (degrees)	β (degrees)	r_a (mm)	r_b (mm)	h (mm)	w (mm)	r_a/h	r_b/h	critical r/h	w/h
Ch4S60	side 1	42.5	56.0	1.79	1.30	0.99	2.86	1.81	1.31	1.31	2.89
		45.0	55.0	1.90	1.34	1.01	2.88	1.88	1.33		2.85
	side 2	40.0	45.5	1.46	1.94	1.03	3.12	1.42	1.88		3.03
		43.0	42.5	1.43	1.93	1.04	3.06	1.38	2.00		2.94
SMI4S60	side 1	28.0	26.0	1.75	1.69	0.74	3.83	2.37	2.28		5.18
		28.0	26.0	1.93	1.41	0.76	3.82	2.54	1.86		5.03
	side 2	30.0	24.0	0.66	2.32	0.65	3.22	1.01	3.57		4.95
		32.5	23.0	0.50	2.29	0.63	3.12	0.79	3.63	0.79	4.95

α, β: flank angles of lugs

r_l, r_r: base radius

h: lug height

w: lug width

Table 2.6 (continued)

Measurements of Lug Properties

Bar Identification		α (degrees)	β (degrees)	r_a (mm)	r_b (mm)	h (mm)	w (mm)	r_a/h	r_b/h	critical r/h	w/h
Ch5S60	side 1	34.0	52.0	1.78	1.43	1.25	3.85	1.42	1.14	0.78	3.08
		33.0	49.0	1.86	1.41	1.27	4.10	1.32	1.11		3.23
	side 2	49.0	53.0	1.15	1.71	1.48	3.69	0.78	1.16		2.49
		48.5	48.0	1.35	1.76	1.52	3.95	0.89	1.16		2.36
Ch5S	Side 1	46.5	45.0	1.26	1.01	1.27	3.82	0.99	0.80	0.80	3.01
		48.0	46.0	1.35	1.15	1.30	3.79	1.04	0.88		2.92
	Side 2	44.0	45.0	1.39	1.25	1.34	3.93	1.04	0.93		2.93
		43.0	47.0	1.52	1.06	1.31	3.80	1.16	0.81		2.90
N5S	side 1	46.5	50.0	1.28	1.07	1.15	4.22	1.11	0.93	0.90	3.67
		43.0	48.0	1.62	1.09	1.21	4.46	1.34	0.90		3.69
	side 2	48.5	32.0	1.02	2.49	1.05	4.79	0.97	2.37		4.56
		46.0	43.0	1.20	1.43	1.06	4.40	1.13	1.35		4.15
FK5S60	Side 1	45.0	48.0	1.36	0.62	1.37	4.42	0.99	0.45	0.45	3.23
		45.5	48.0	0.94	0.74	1.35	4.47	0.70	0.55		3.31
	Side 2	41.5	45.0	1.30	0.95	1.32	4.79	0.98	0.72		3.63
		43.0	53.0	1.50	0.66	1.35	4.58	1.11	0.49		3.39

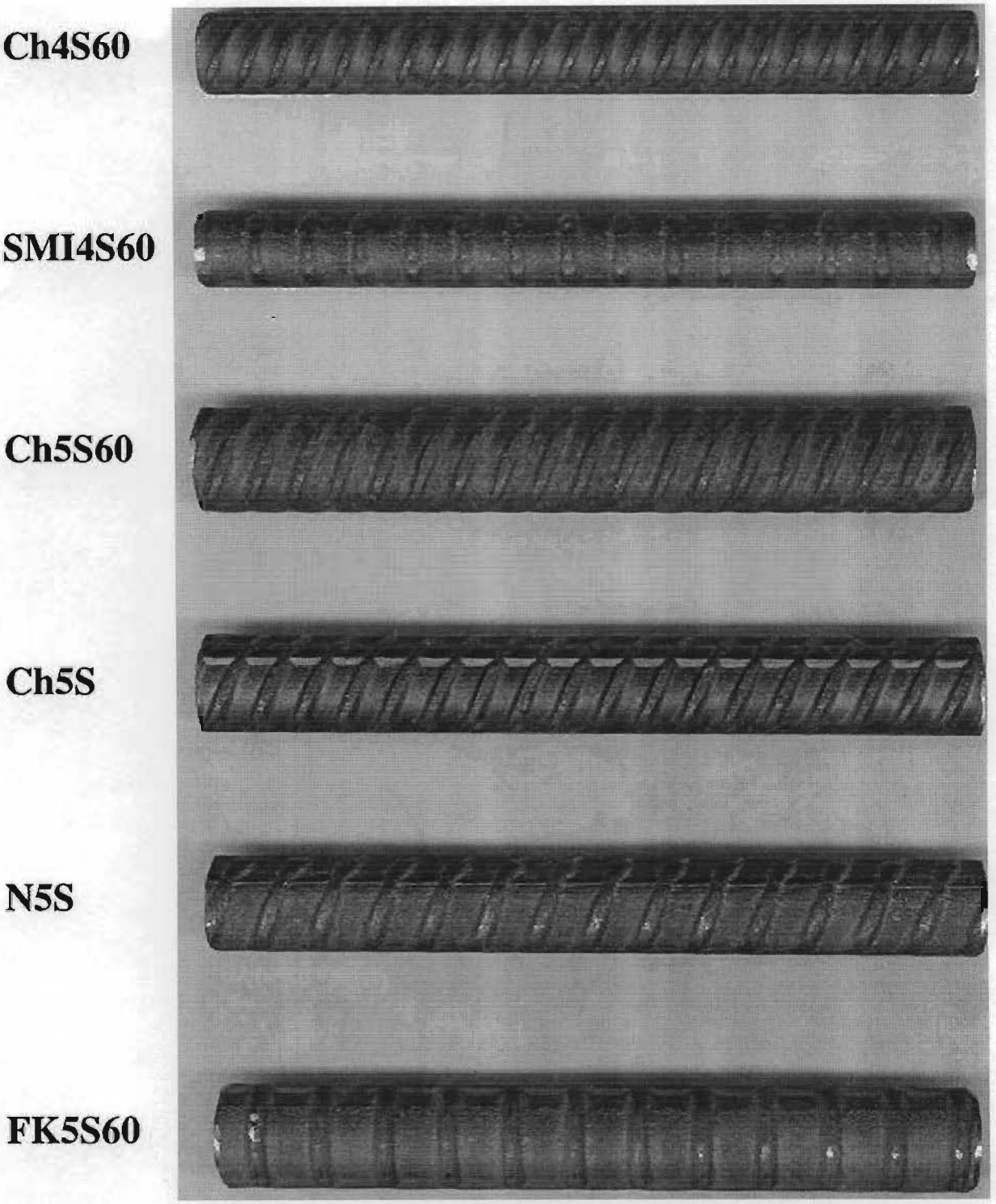

Fig. 2.1 Test Bars

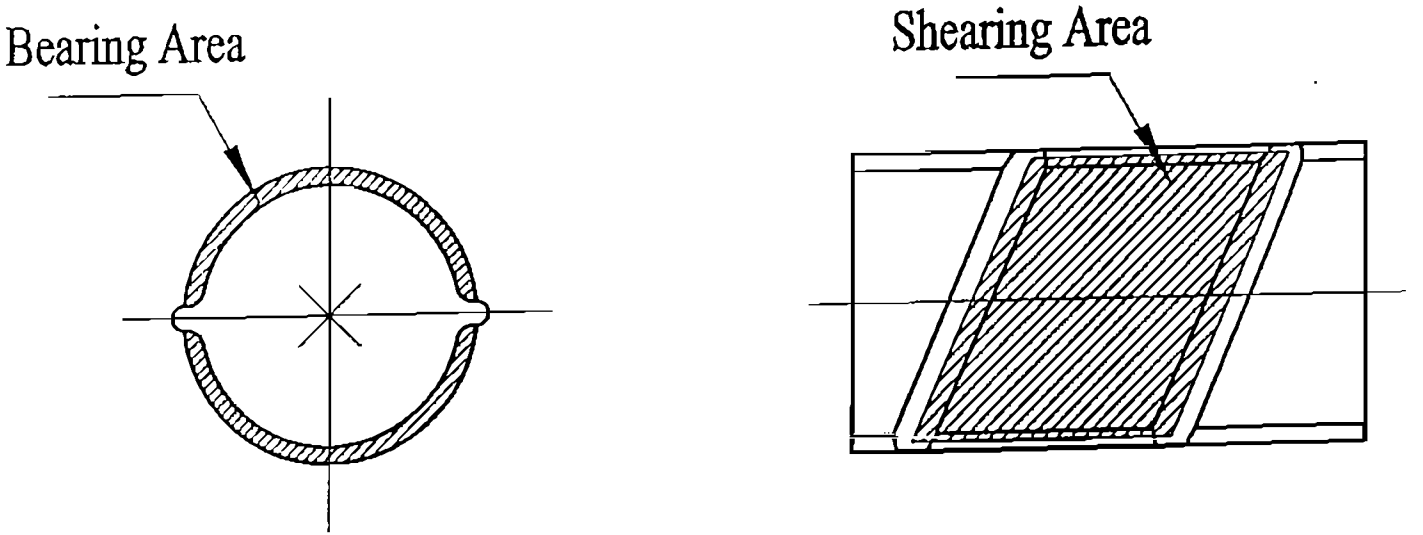

$$R_r = \frac{\text{Bearing Area}}{\text{Shearing Area}} = \frac{h_r}{s_r}\left(1 - \frac{\sum \text{gaps}}{p}\right)$$

Fig. 2.2 Schematic Illustration of Relative Rib Area (see Eq. 2.1)

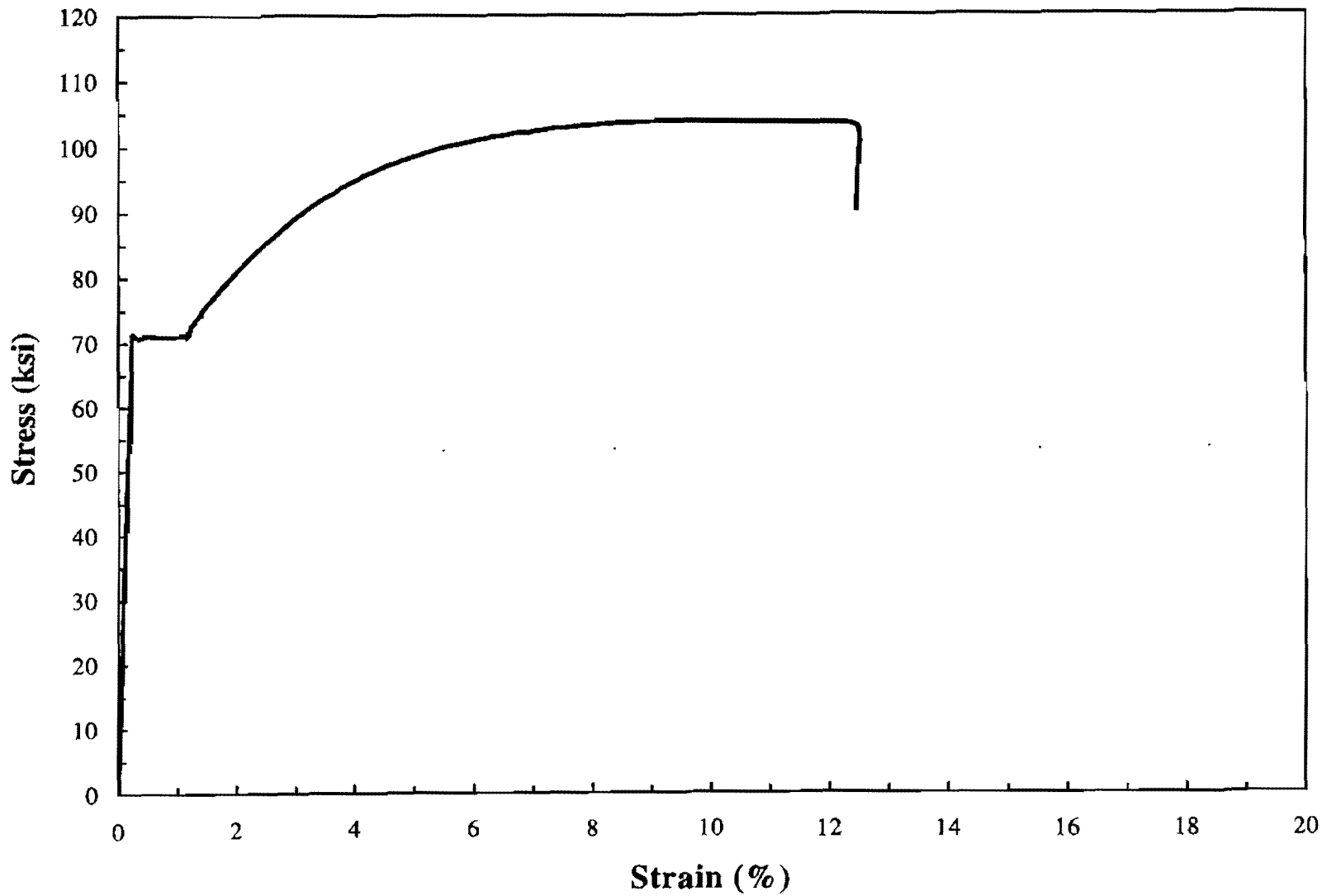

Fig. 2.3 Typical Stress-Strain Curve for Ch4S60 Bars

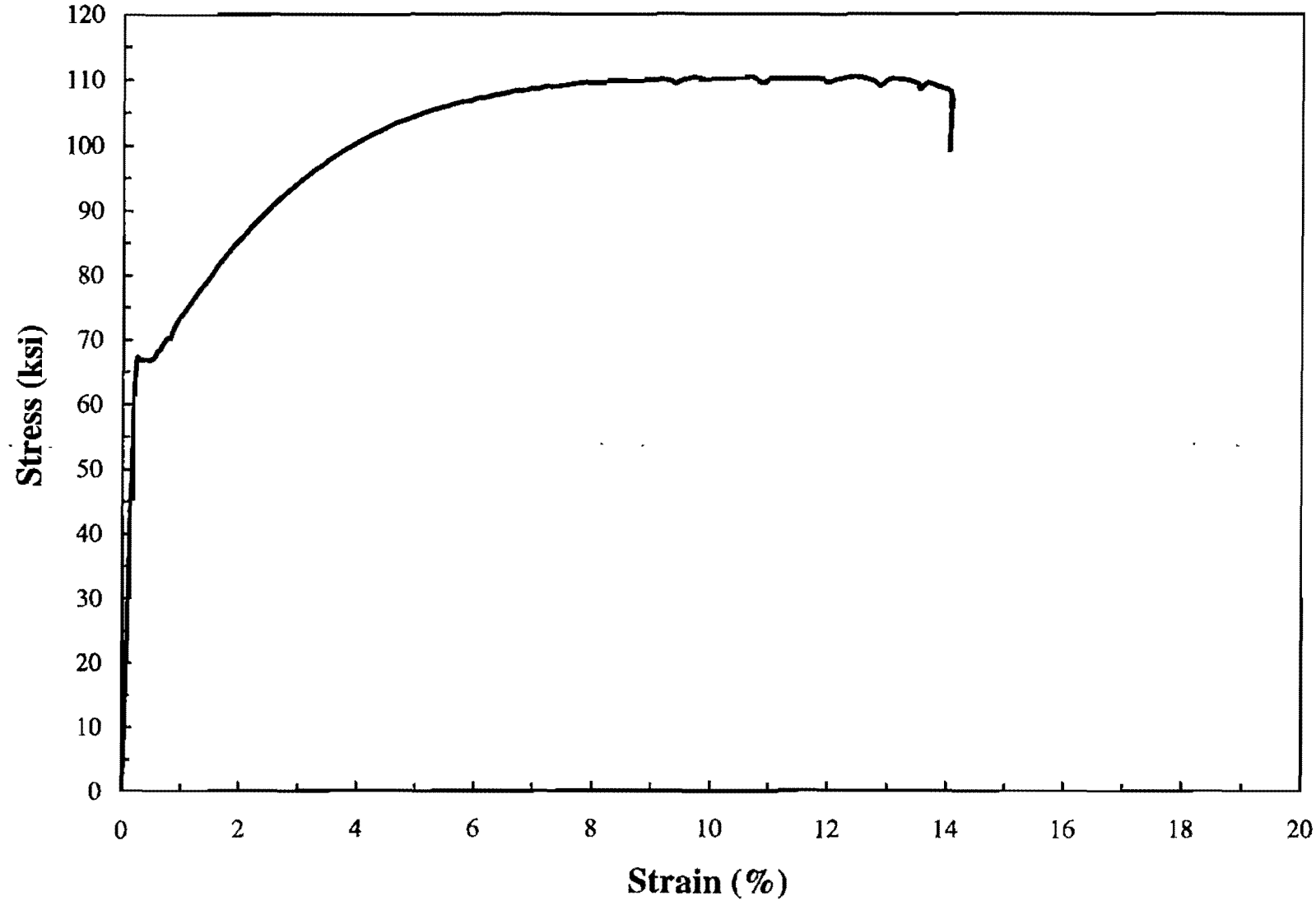

Fig. 2.4 Typical Stress-Strain Curve for SMI4S60 Bars

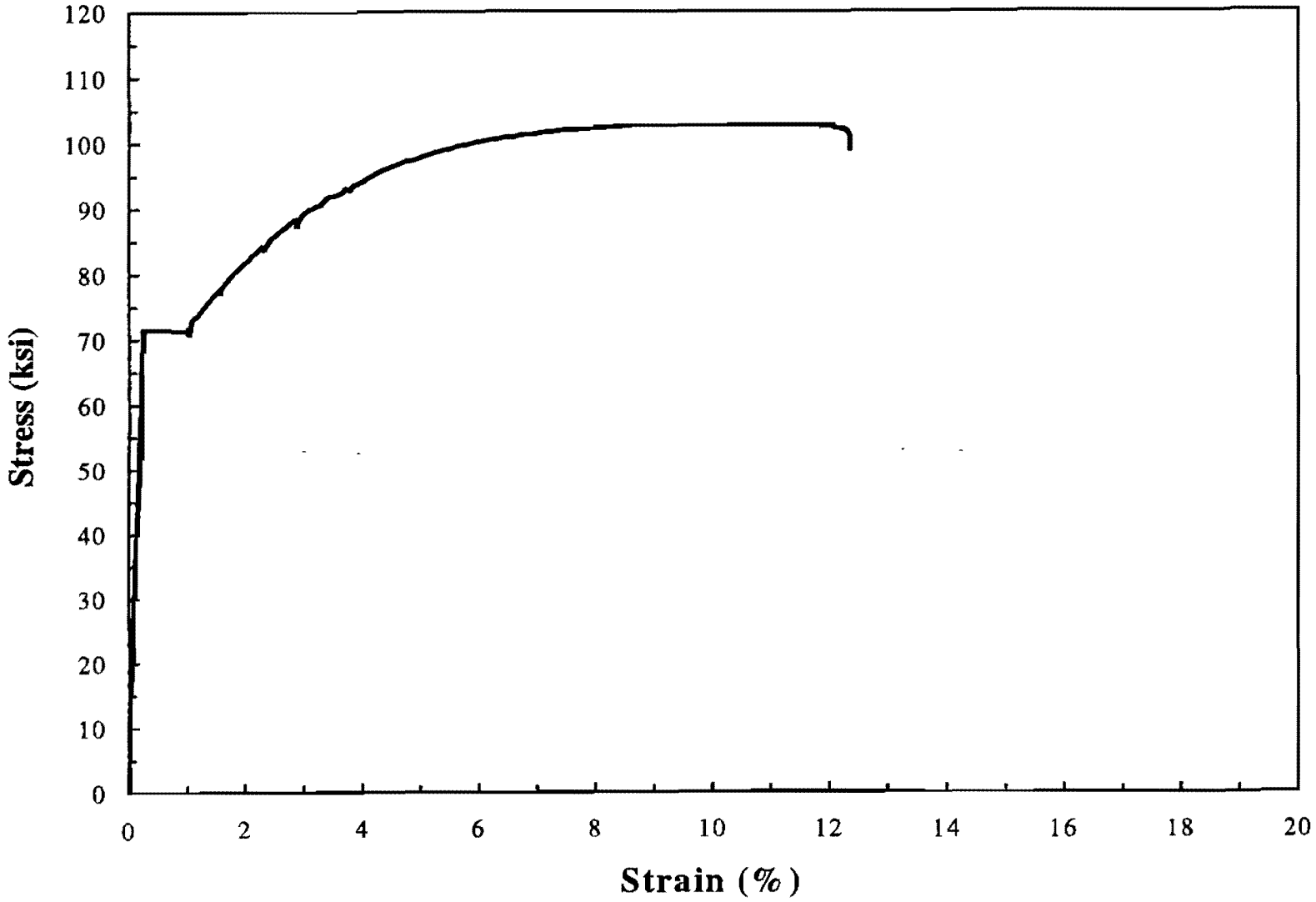

Fig. 2.5 Typical Stress-Strain Curve for Ch5S60 Bars

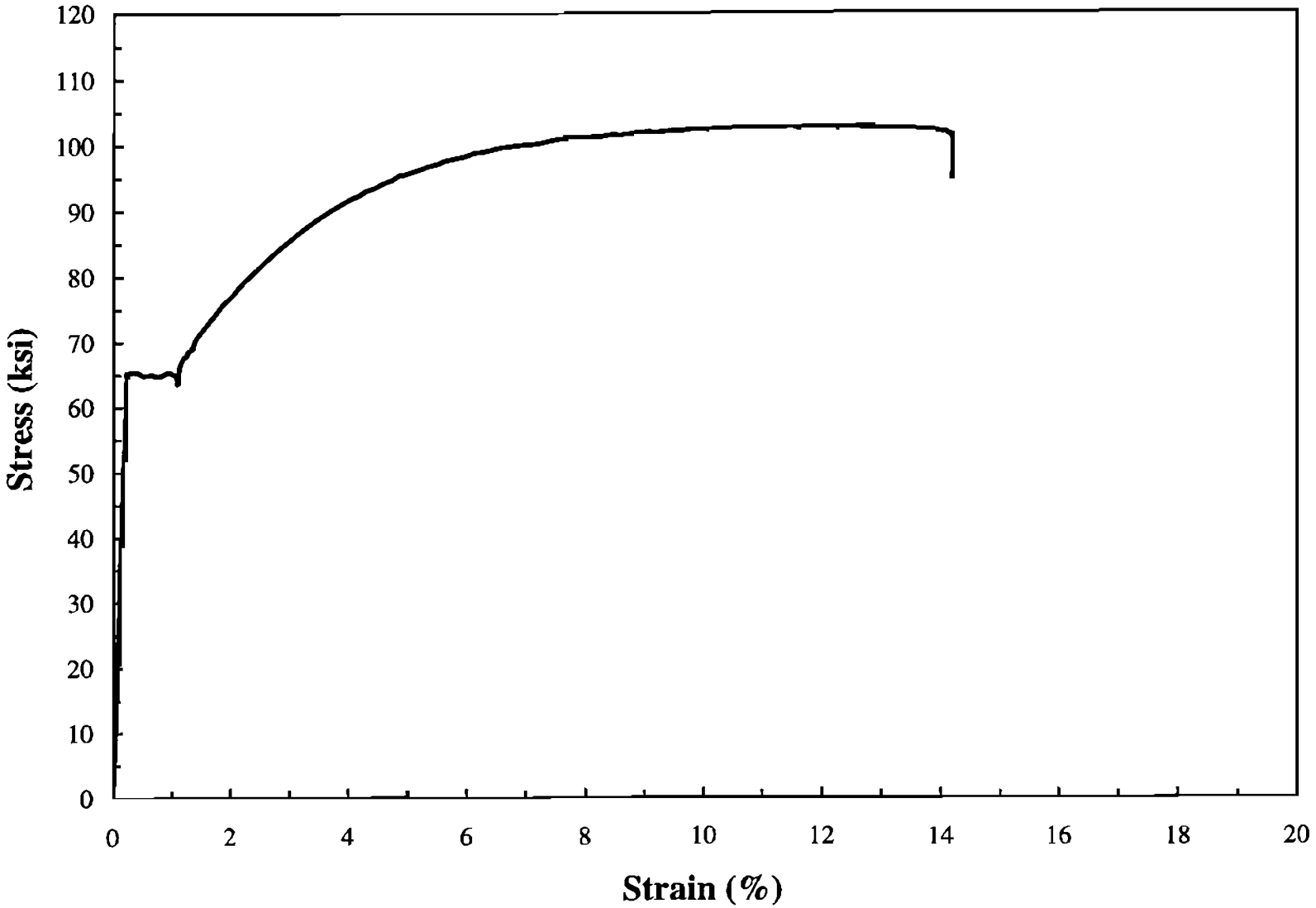

Fig. 2.6 Typical Stress-Strain Curve for Ch5S Bars

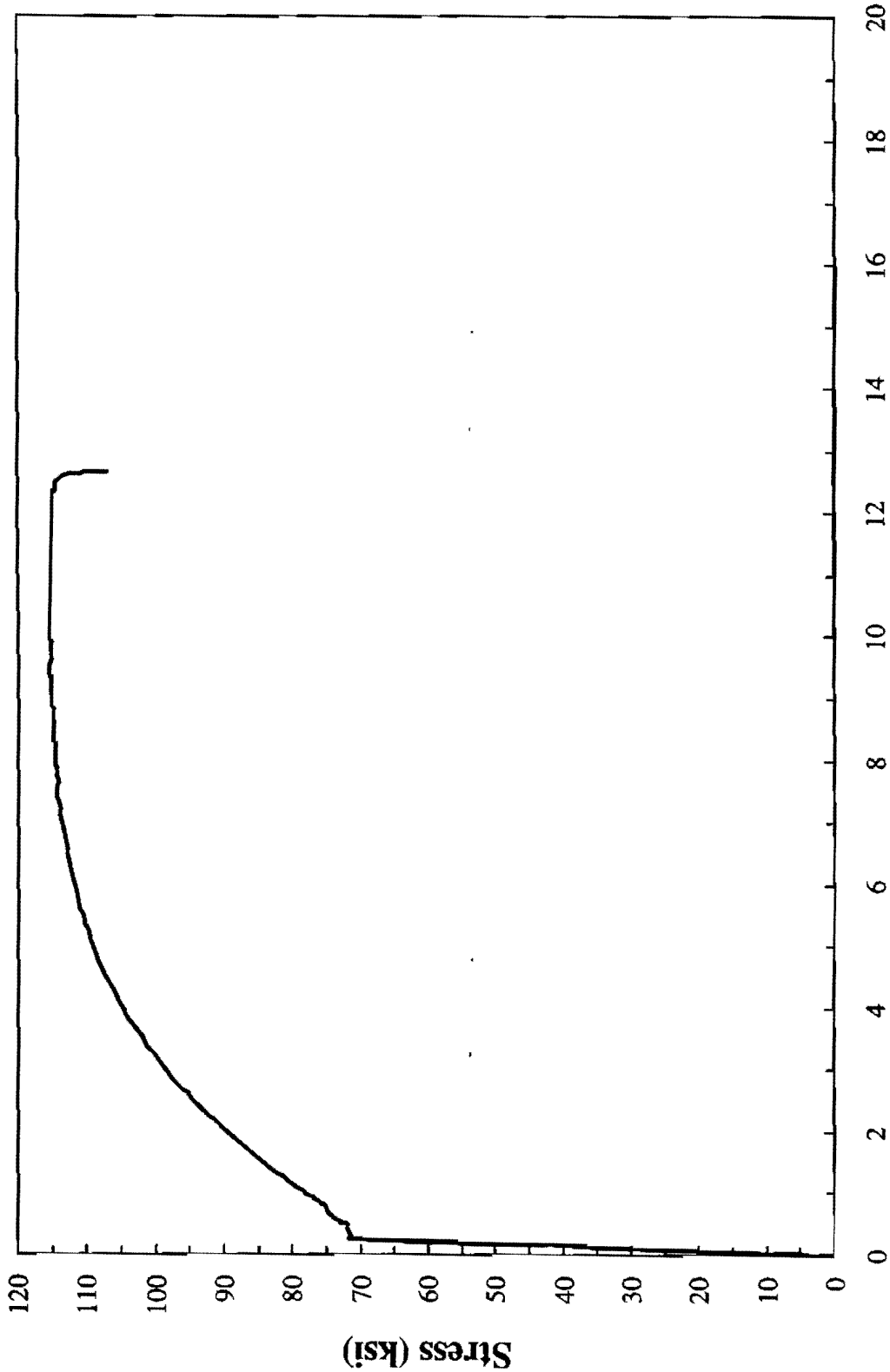

Fig. 2.7 Typical Stress-Strain Curve for N5S Bars

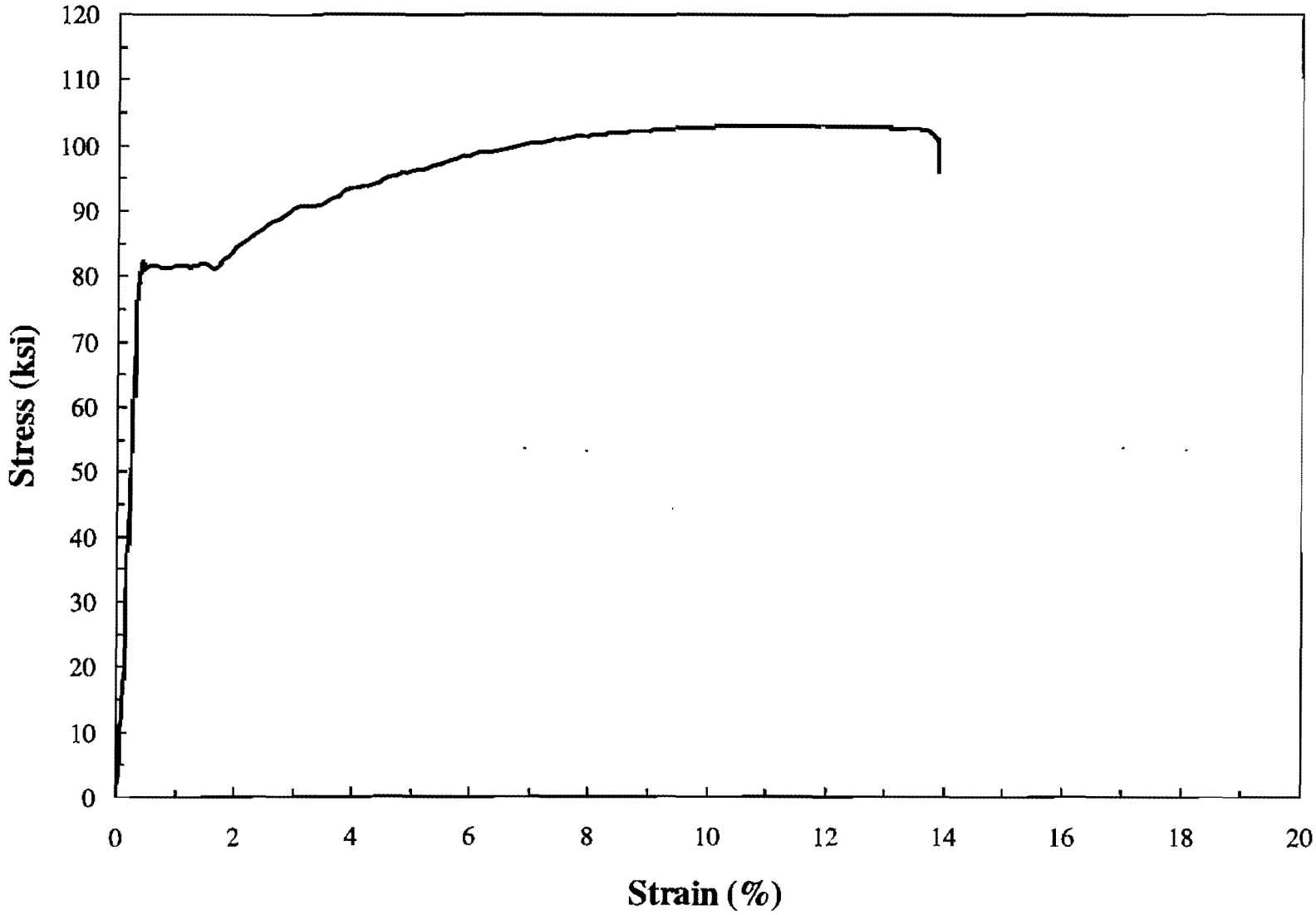

Fig. 2.8 Typical Stress-Strain Curve for FK5S60 Bars

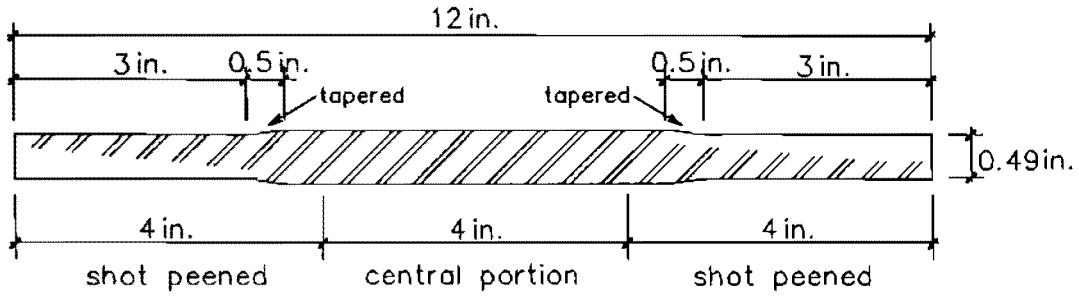

No.4 bar specimen

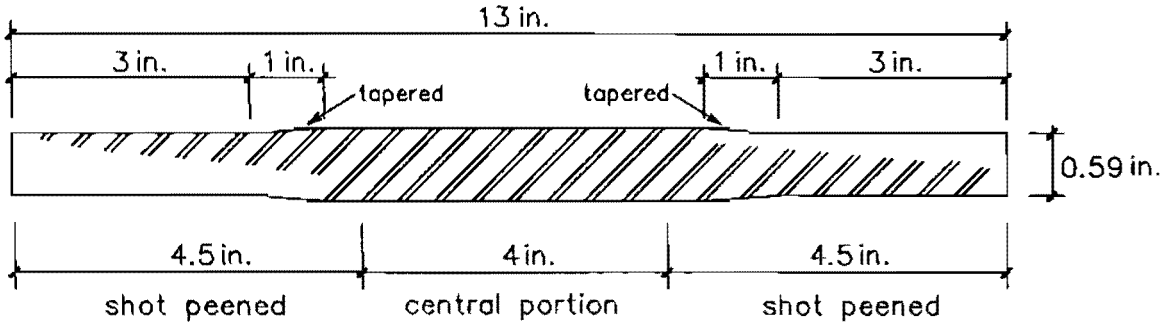

No.5 bar specimen

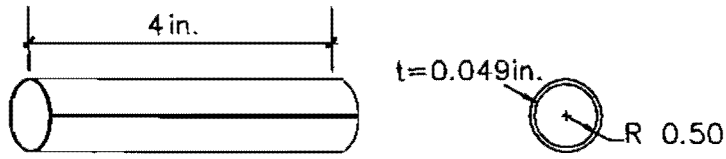

Type K copper tubing

Fig. 2.9 Specimen Prepared for Fatigue Tests

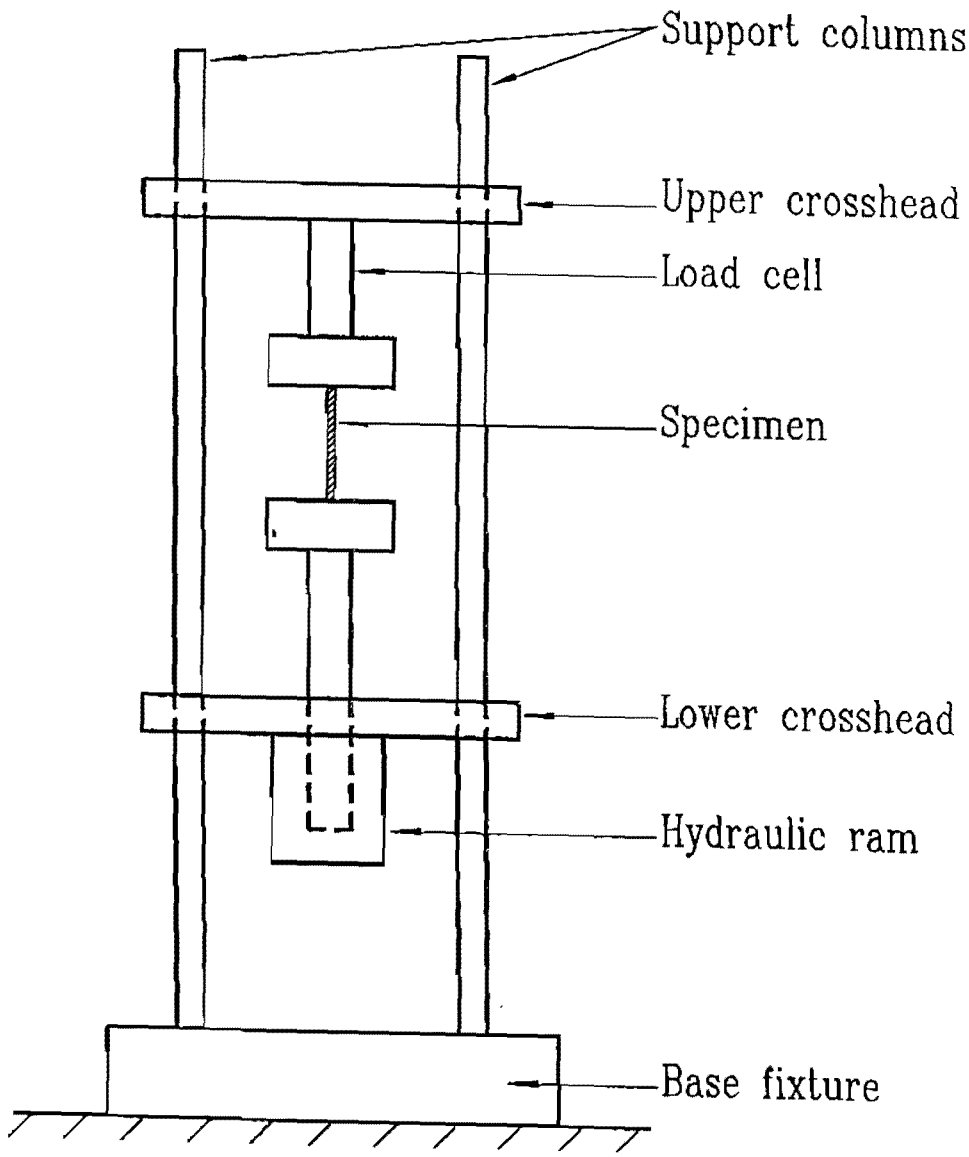

Fig. 2.10 Schematic of Test Set-Up

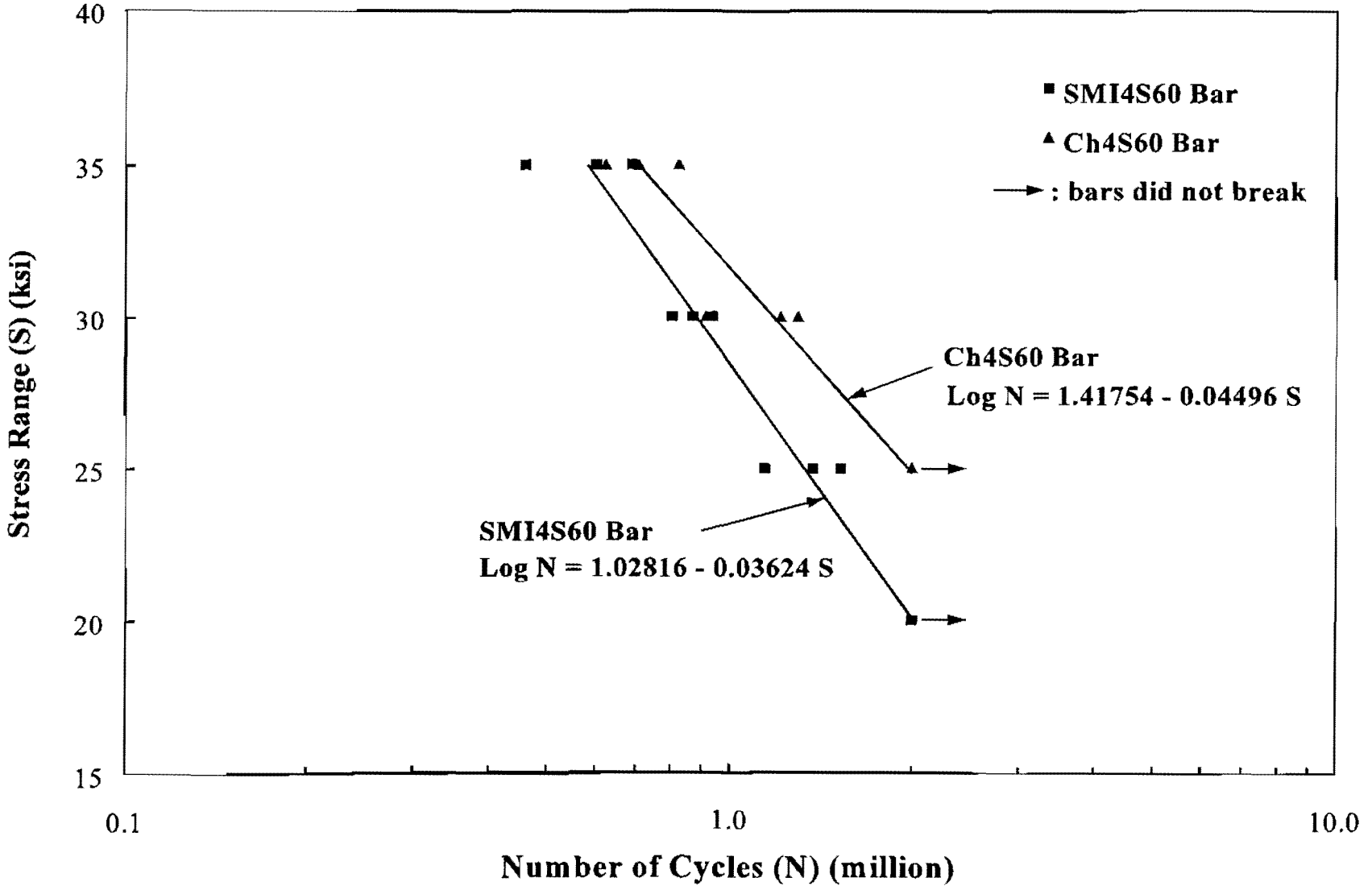

Fig. 2.11 S-N Curves for No. 4 (13 mm) Bars

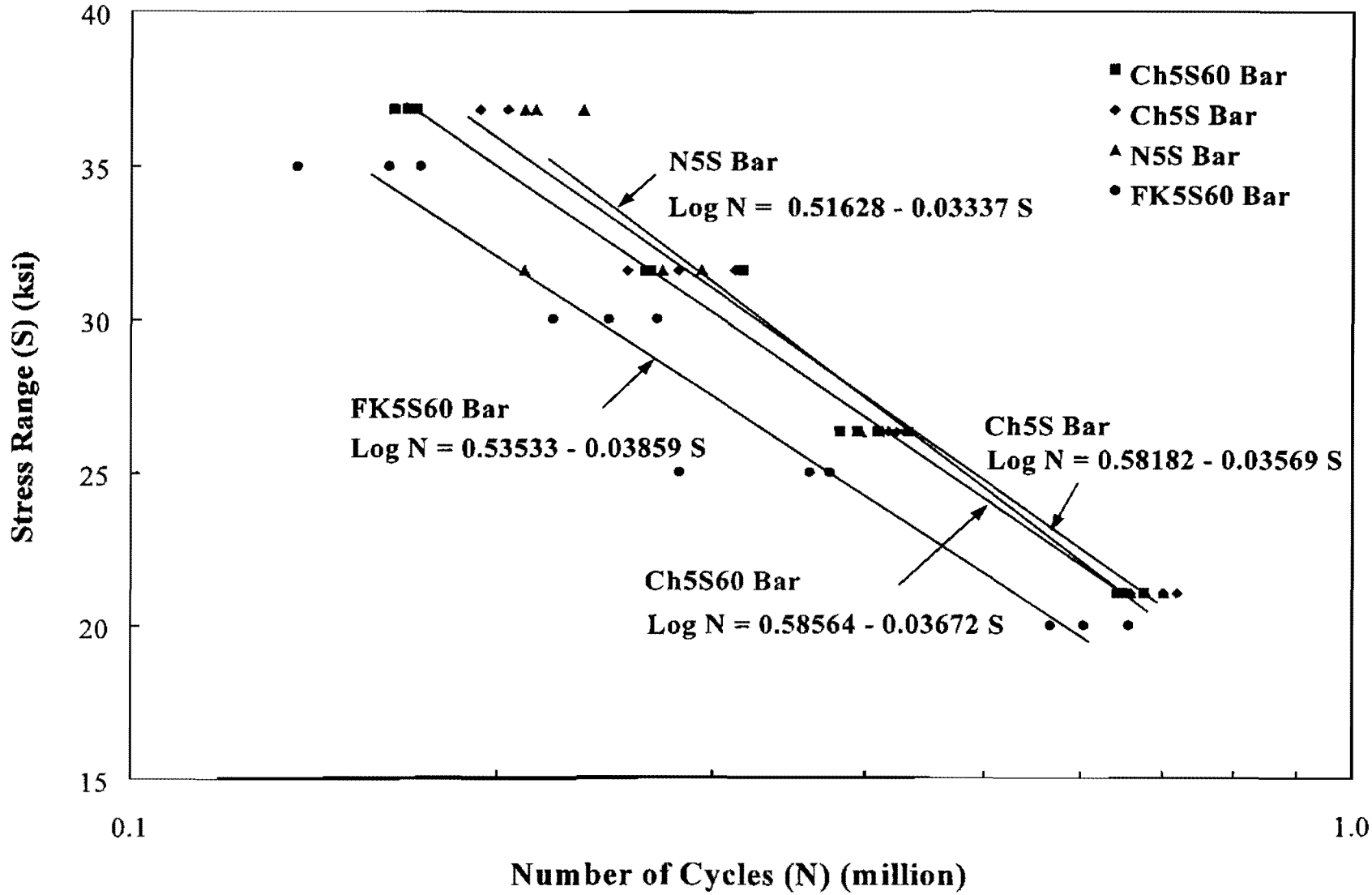

Fig. 2.12 S-N Curves for No. 5 (16 mm) Bars

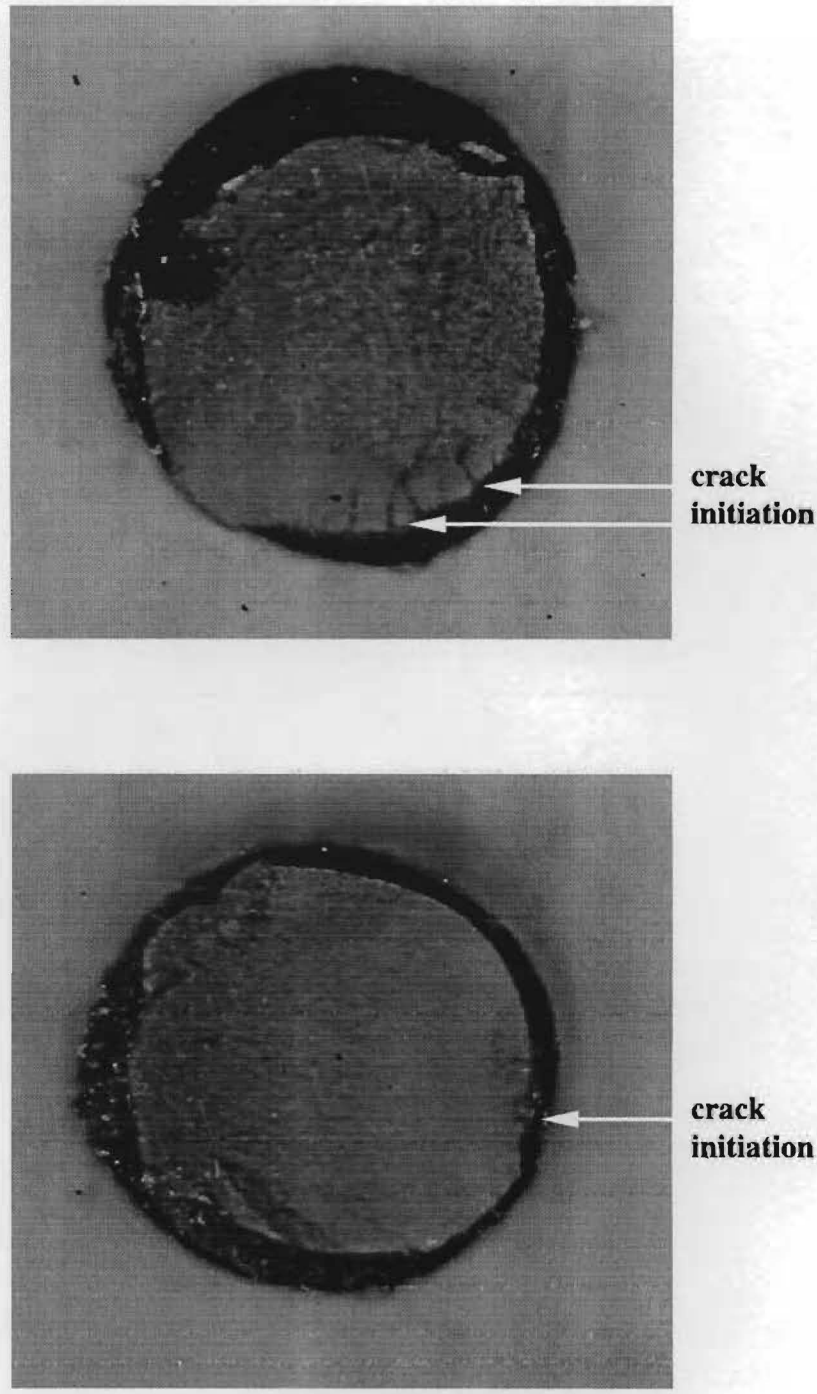

Fig. 2.13 Fatigue Crack Surfaces on Ch4S60 Bars

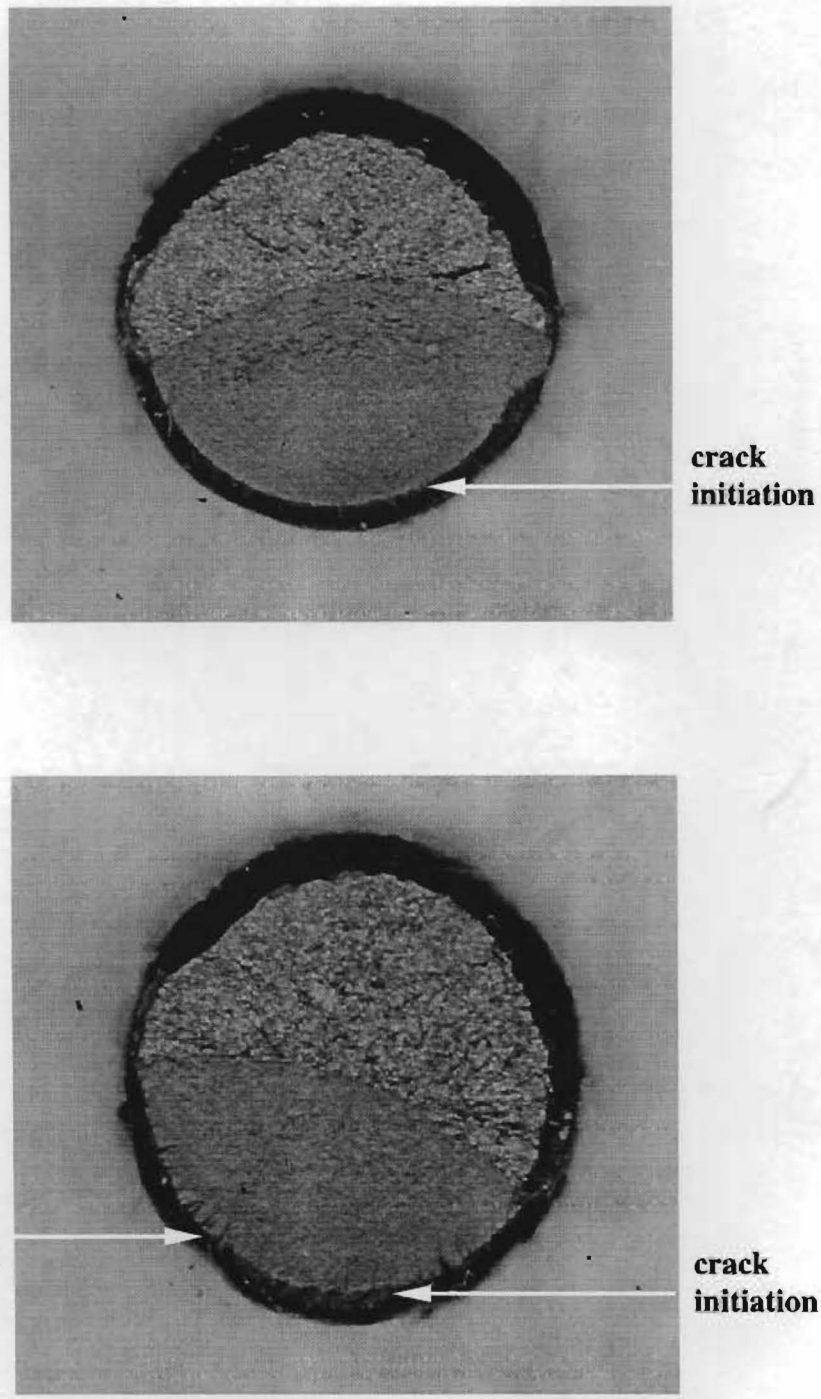

Fig. 2.14 Fatigue Crack Surfaces on SMI4S60 Bars

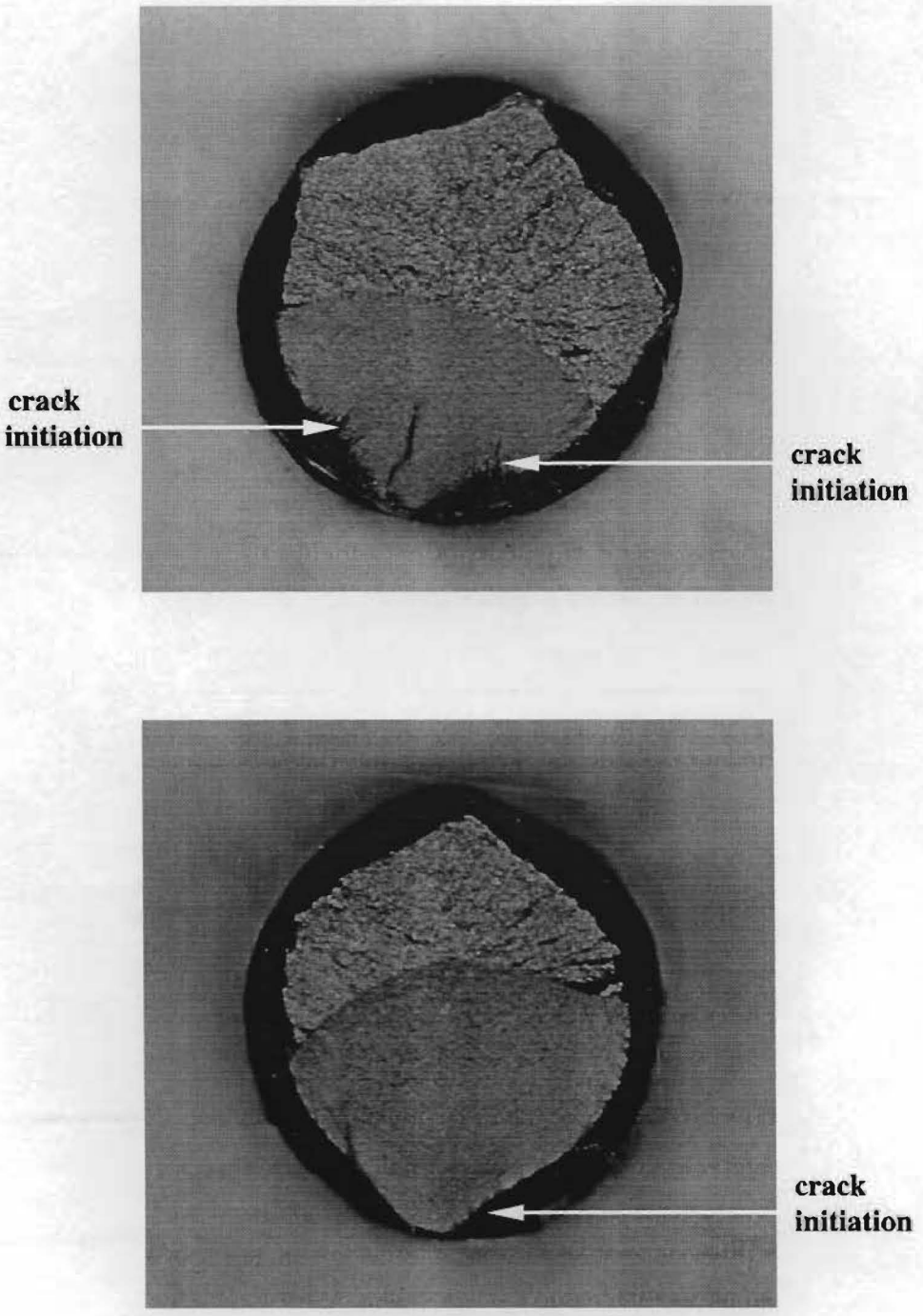

Fig. 2.15 Fatigue Crack Surfaces on Ch5S60 Bars

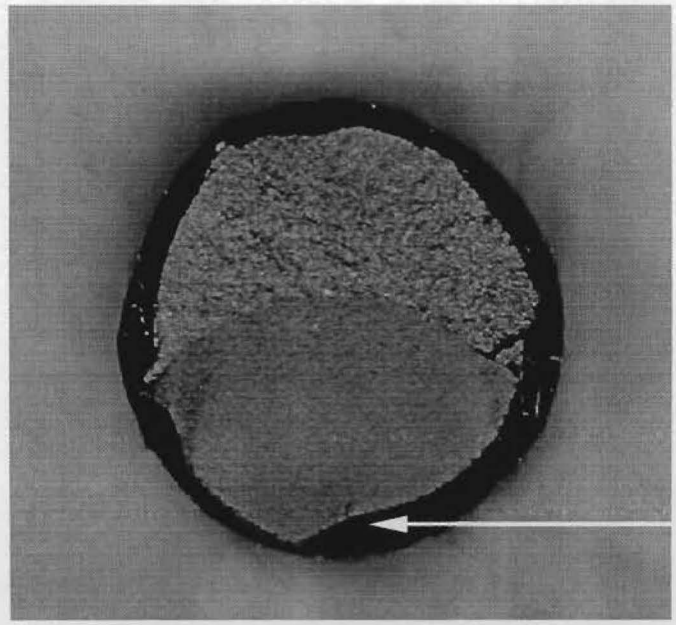

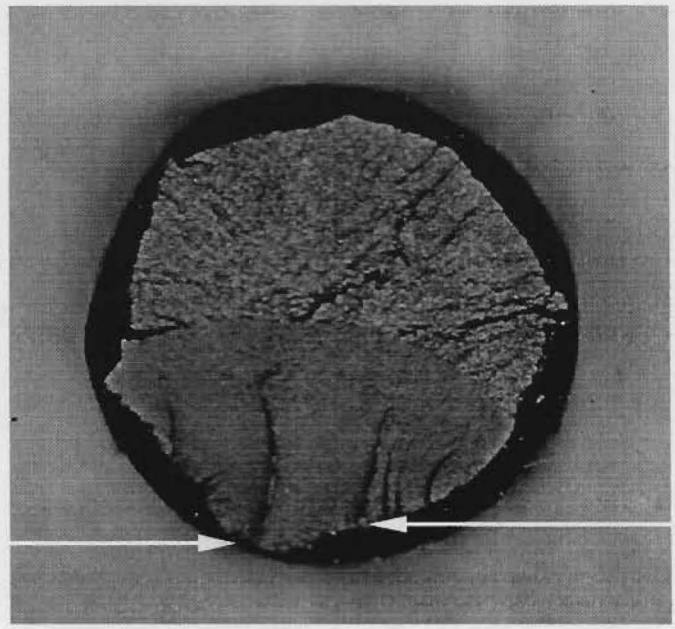

Fig. 2.16 Fatigue Crack Surfaces on Ch5S Bars

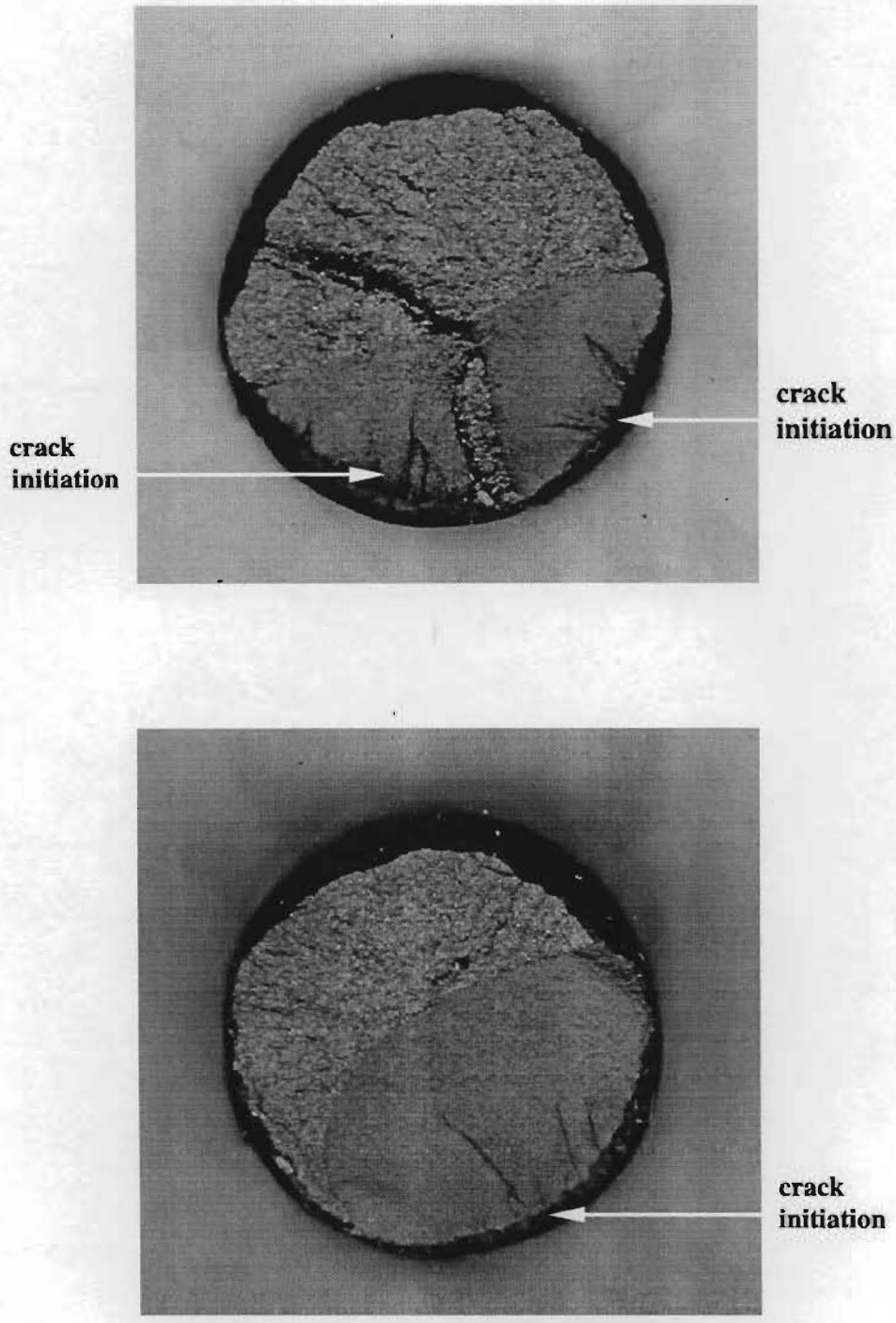

Fig. 2.17 Fatigue Crack Surfaces on N5S Bars

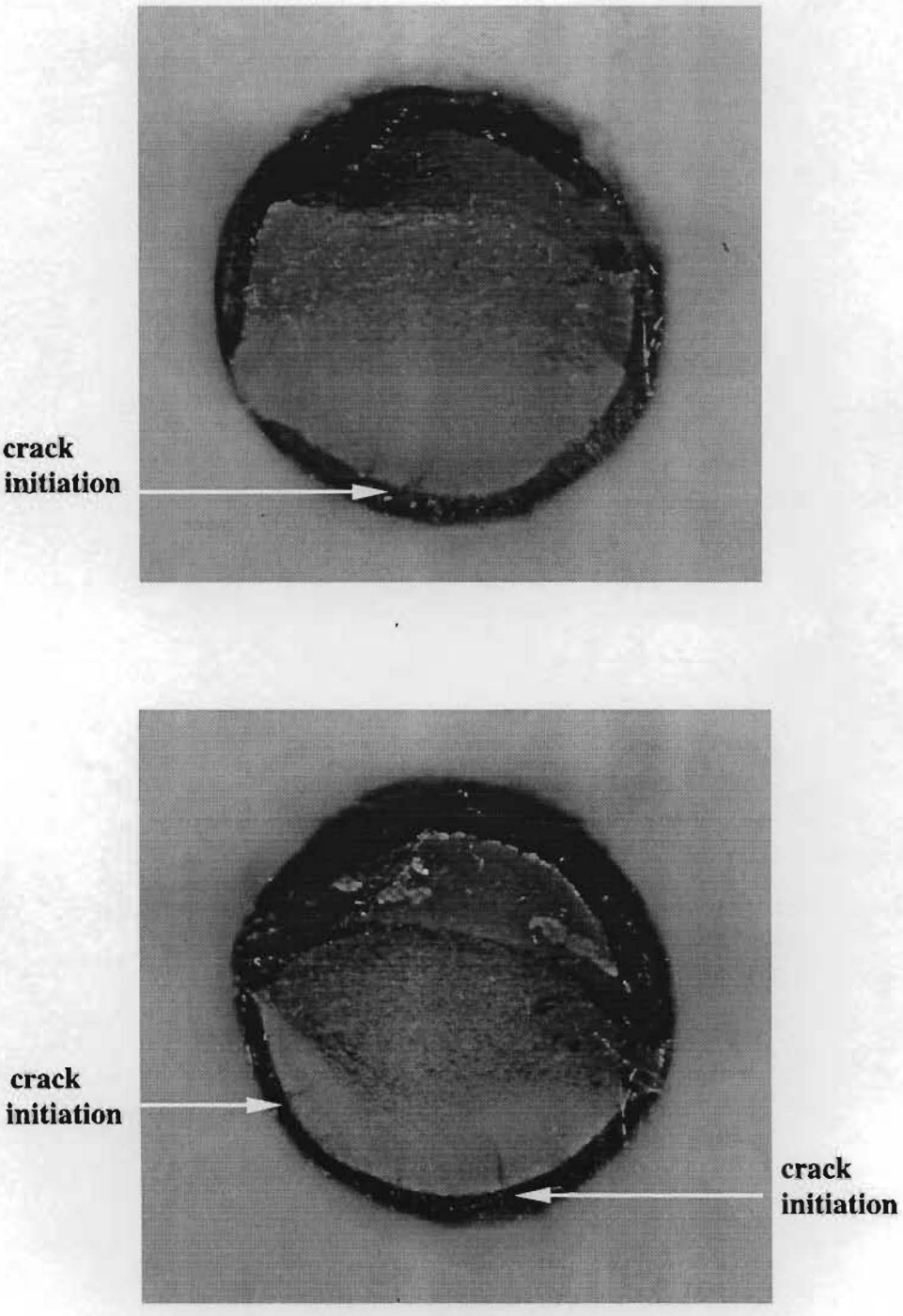

Fig. 2.18 Fatigue Crack Surfaces on FK5S60 Bars

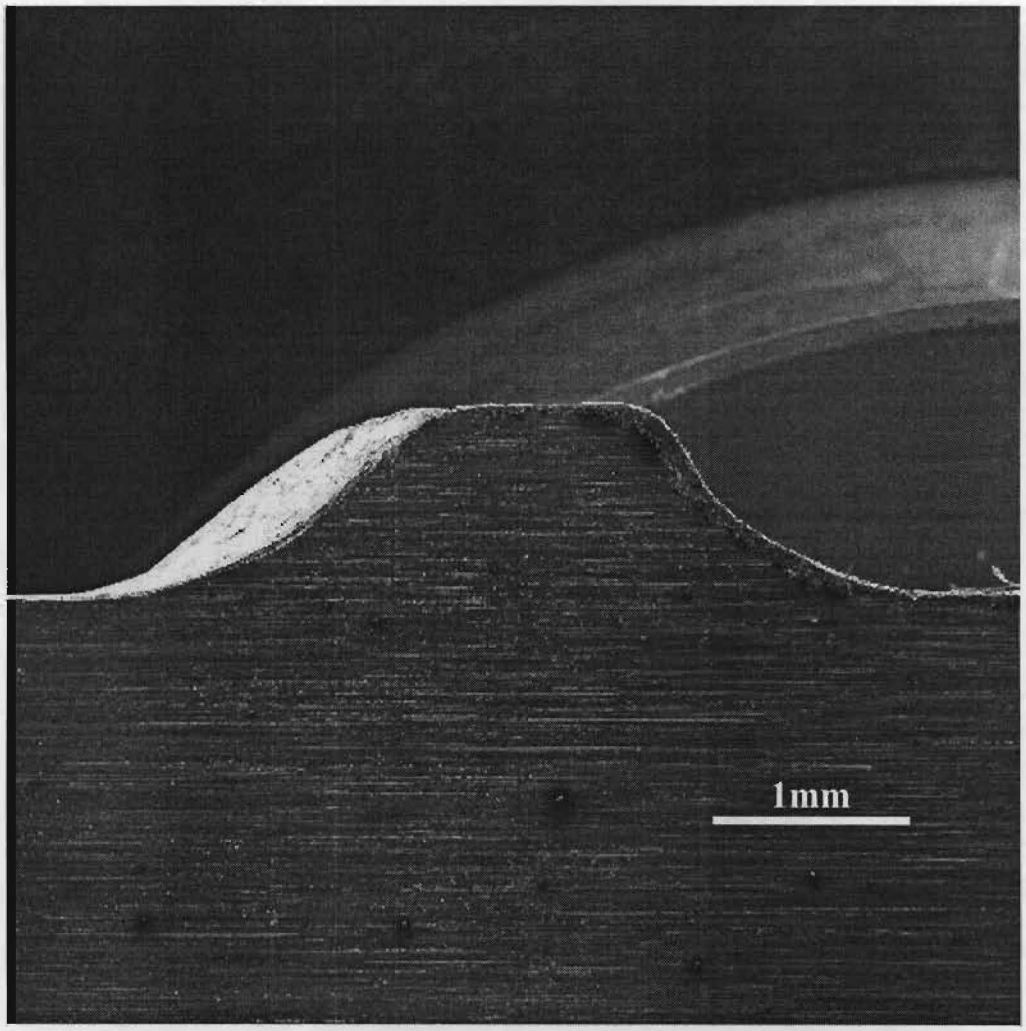

Fig. 2.19 Scanning Electron Microscope Image of a Lug on a Ch4S60 Bar

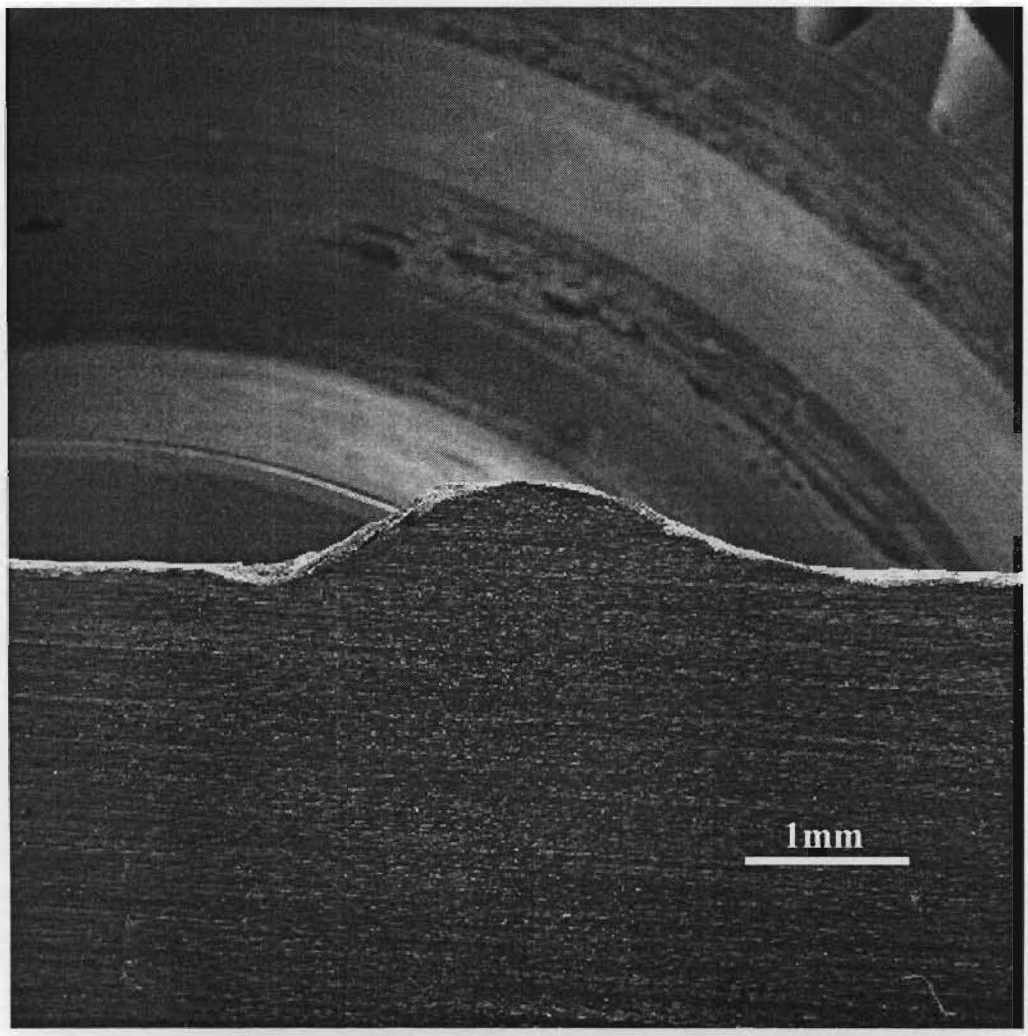

Fig. 2.20 Scanning Electron Microscope Image of a Lug on a SMI4S60 Bar

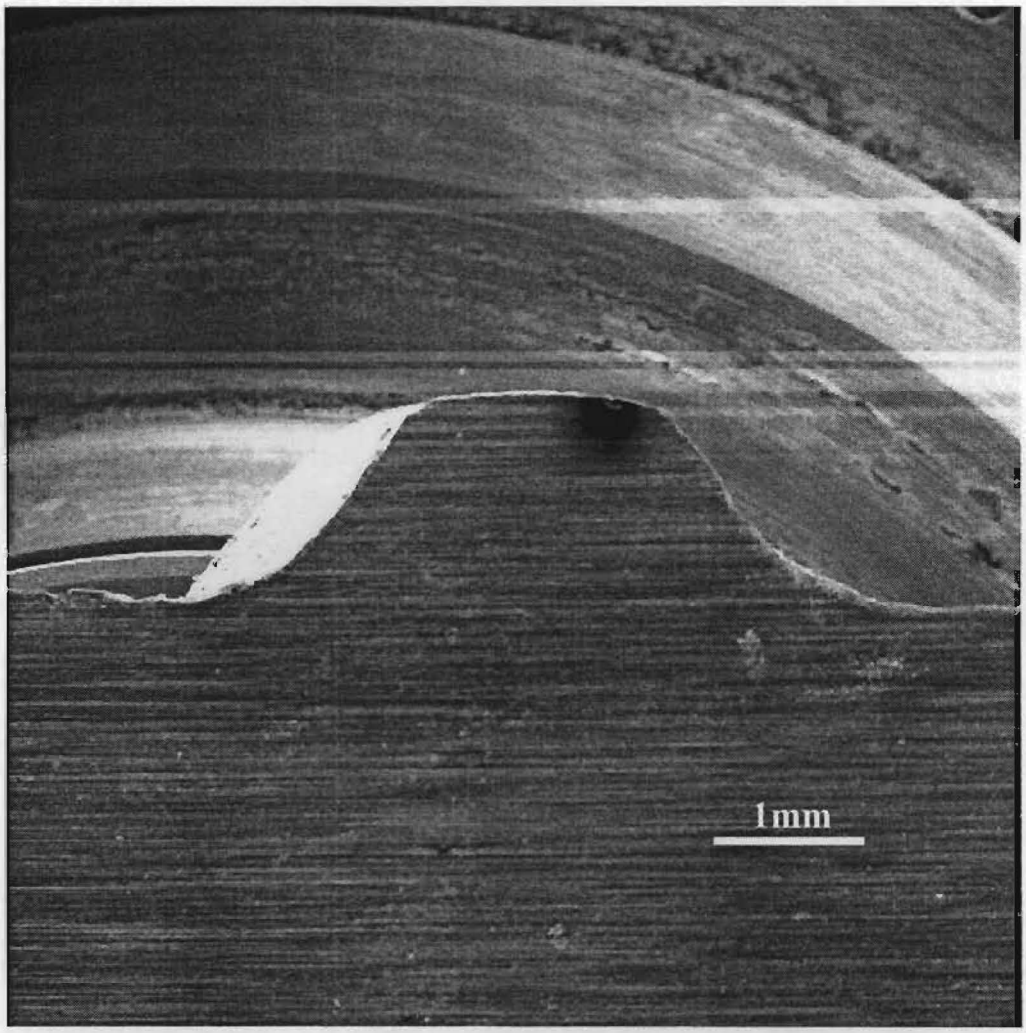

Fig. 2.21 Scanning Electron Microscope Image of a Lug on a Ch5S60 Bar

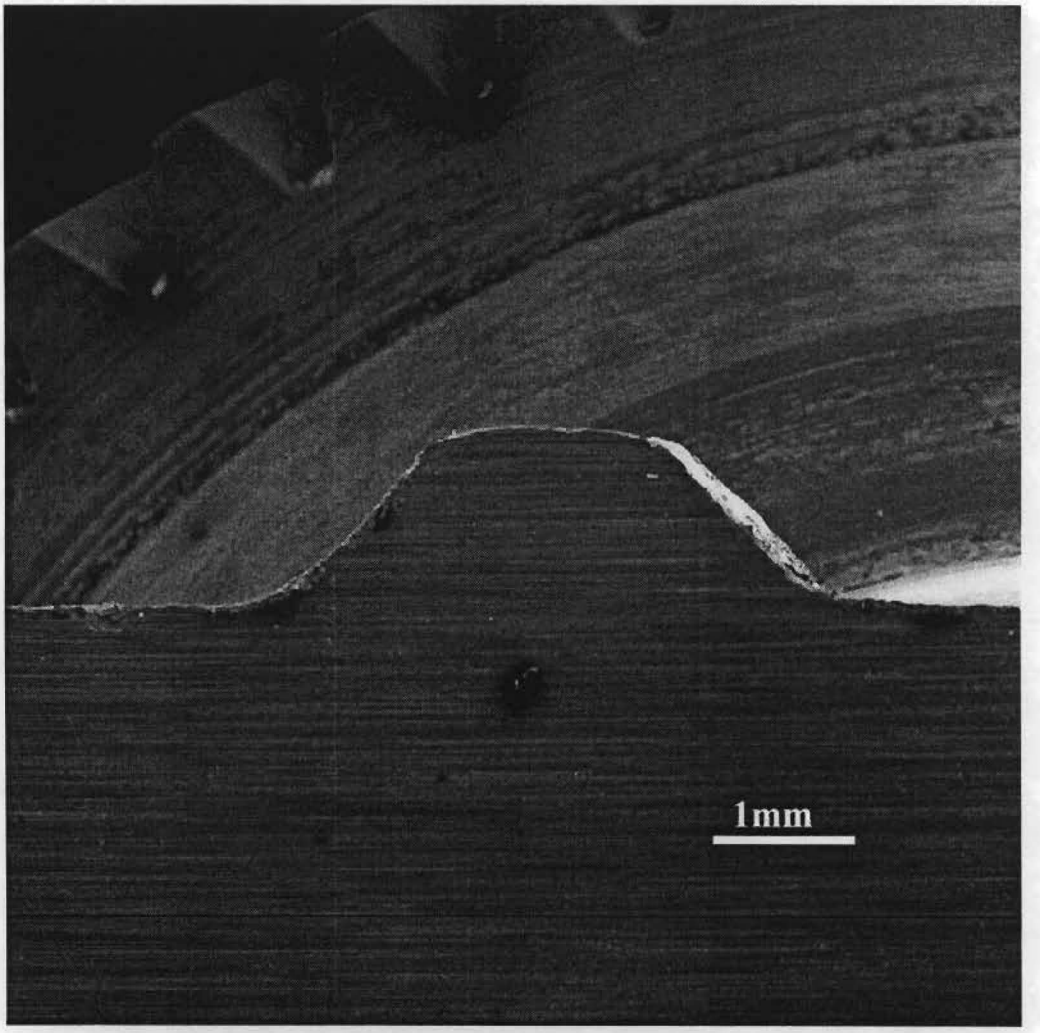

Fig. 2.22 Scanning Electron Microscope Image of a Lug on a Ch5S Bar

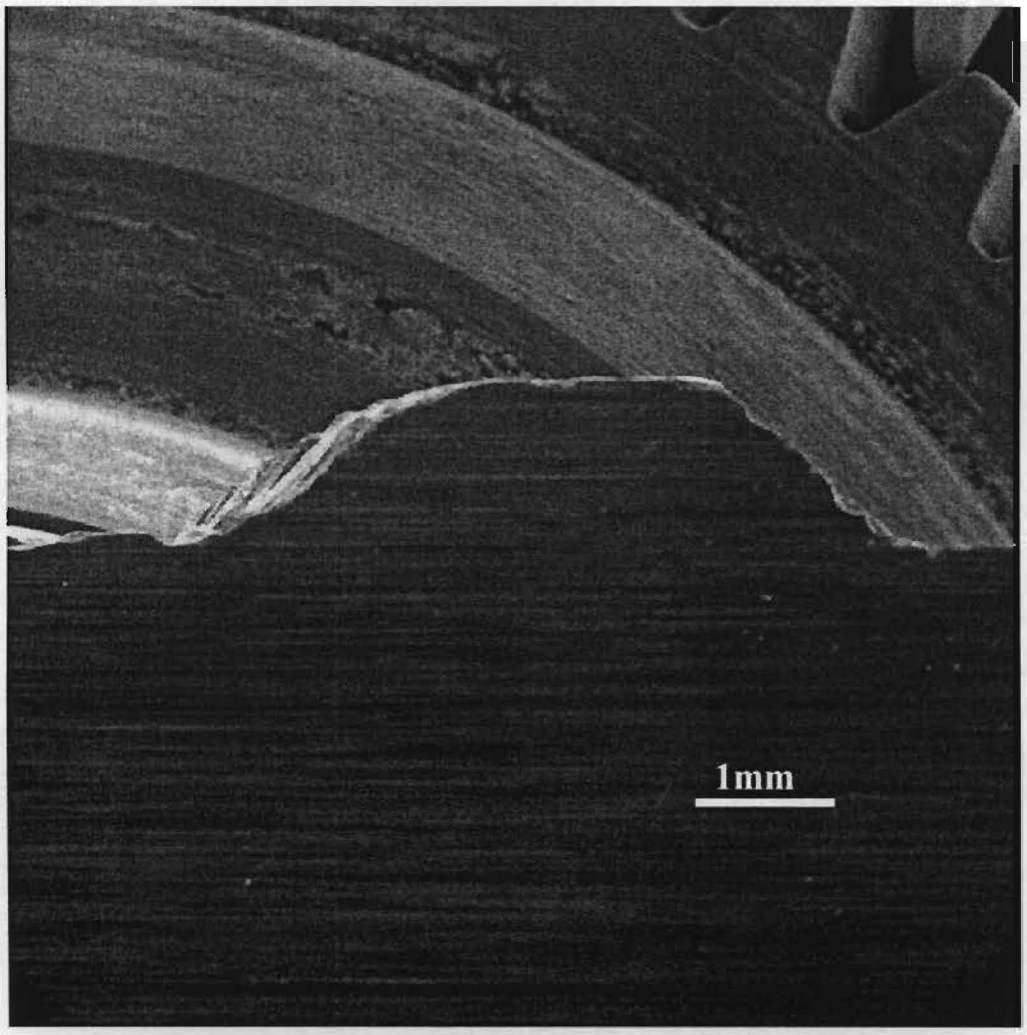

Fig. 2.23 Scanning Electron Microscope Image of a Lug on a N5S Bar

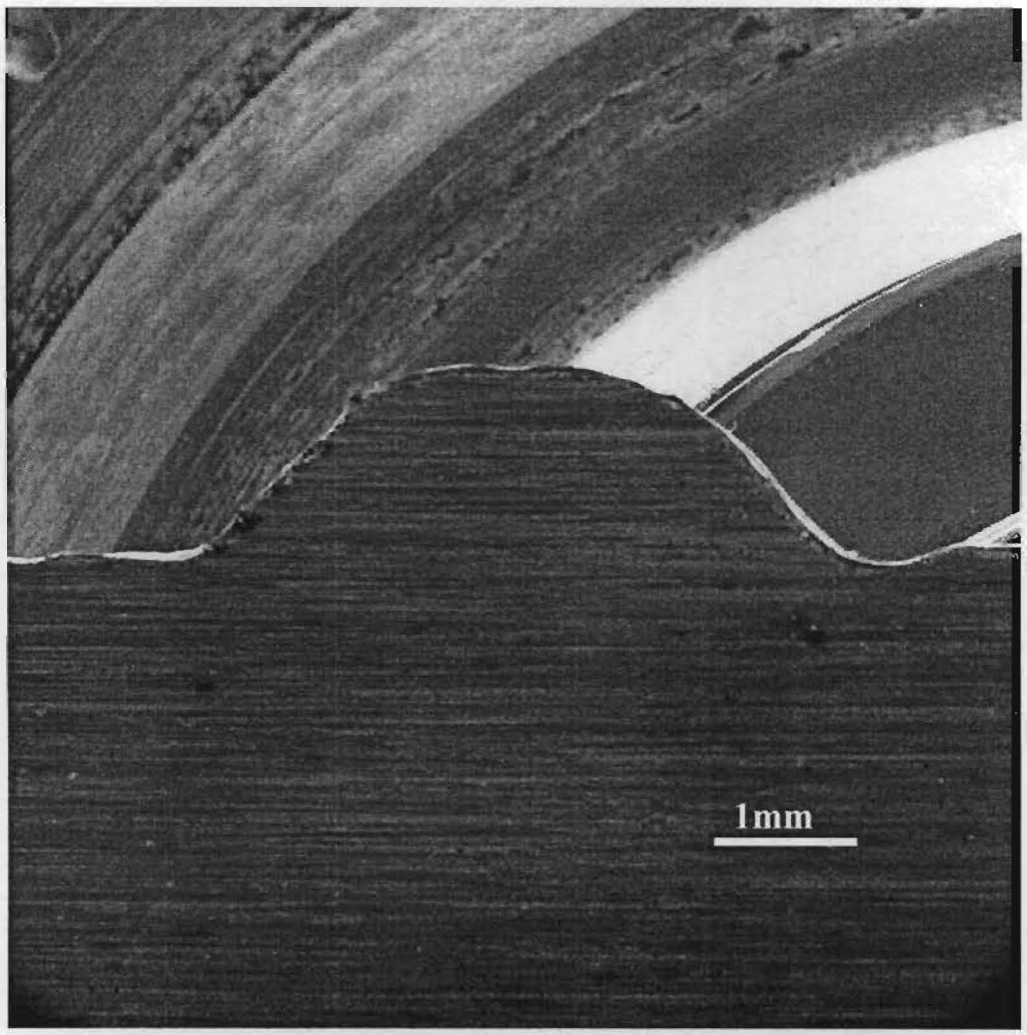

Fig. 2.24 Scanning Electron Microscope Image of a Lug on a FK5S60 Bar

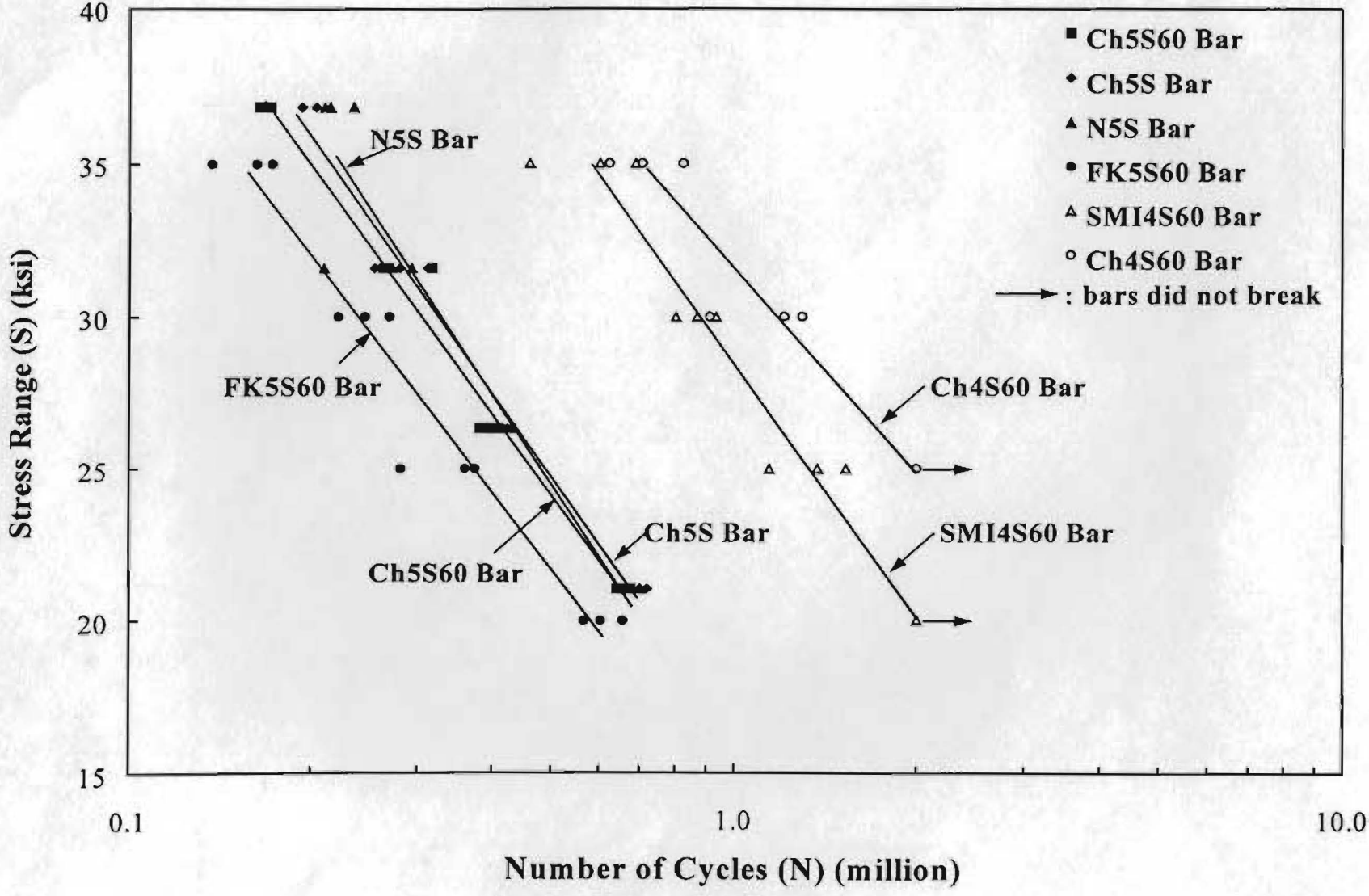

Fig. 3.1 Effect of Bar Diameter

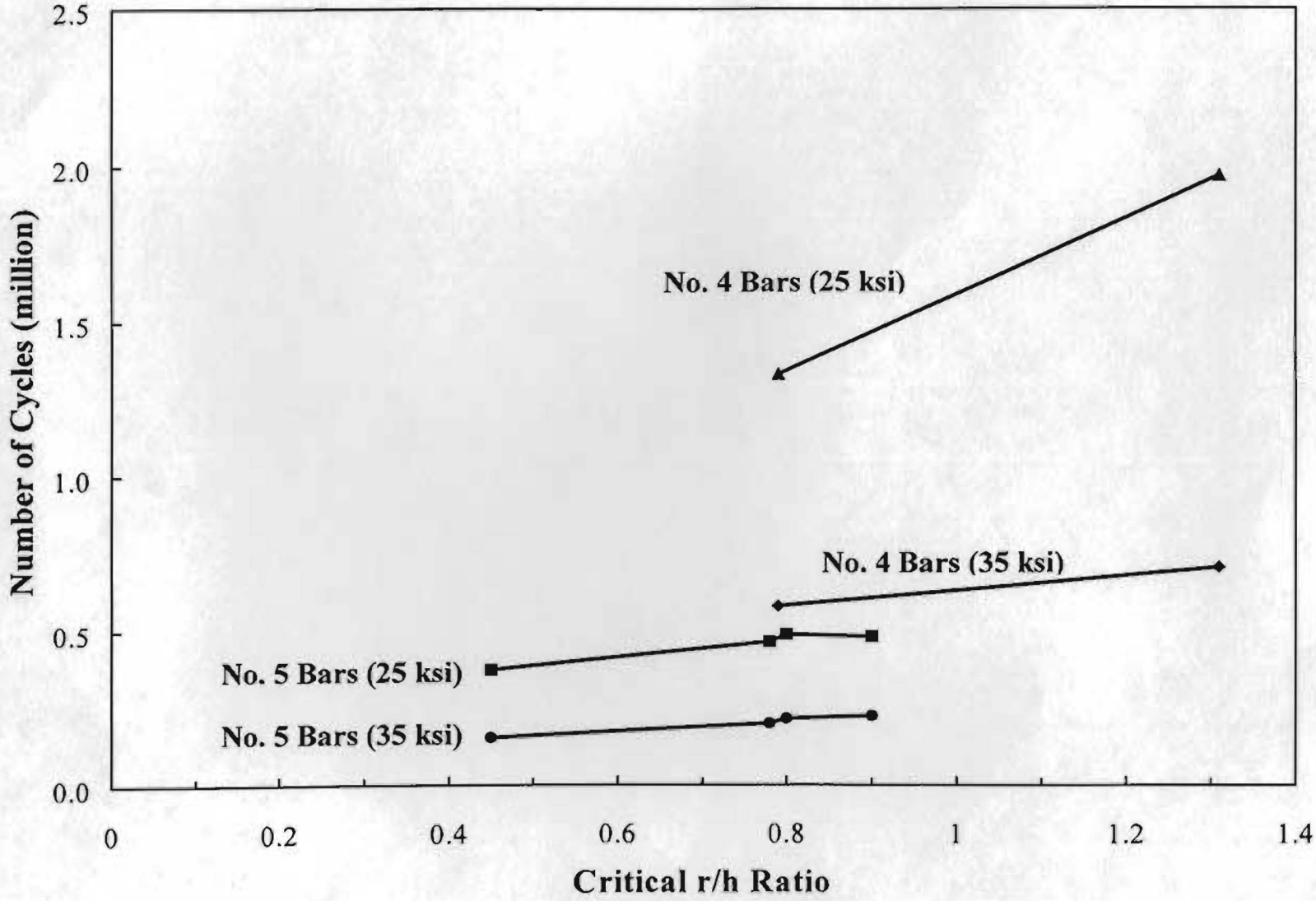

Fig. 3.2 Effect of Critical r/h Ratios

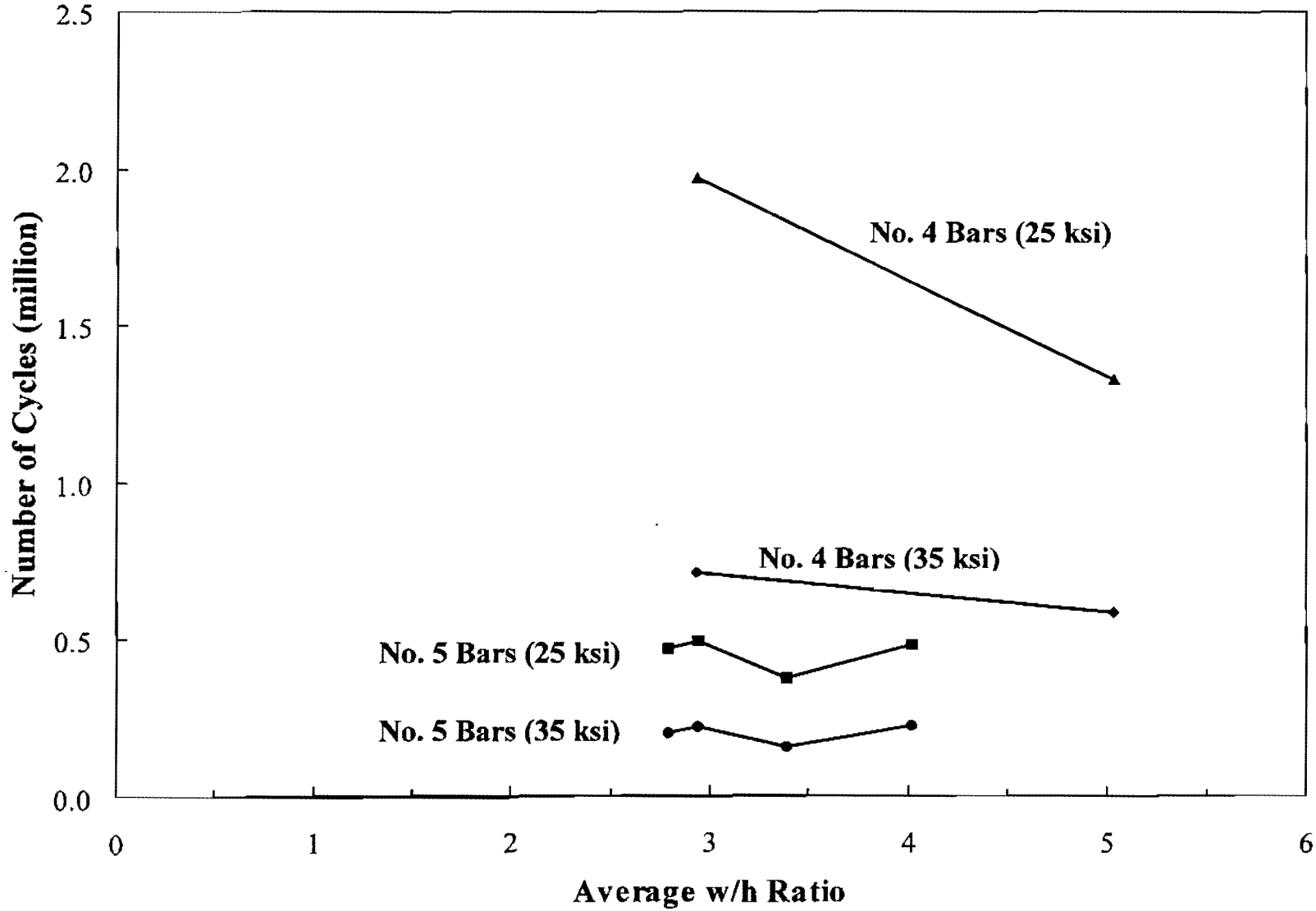

Fig. 3.3 Effect of Average w/h Ratios

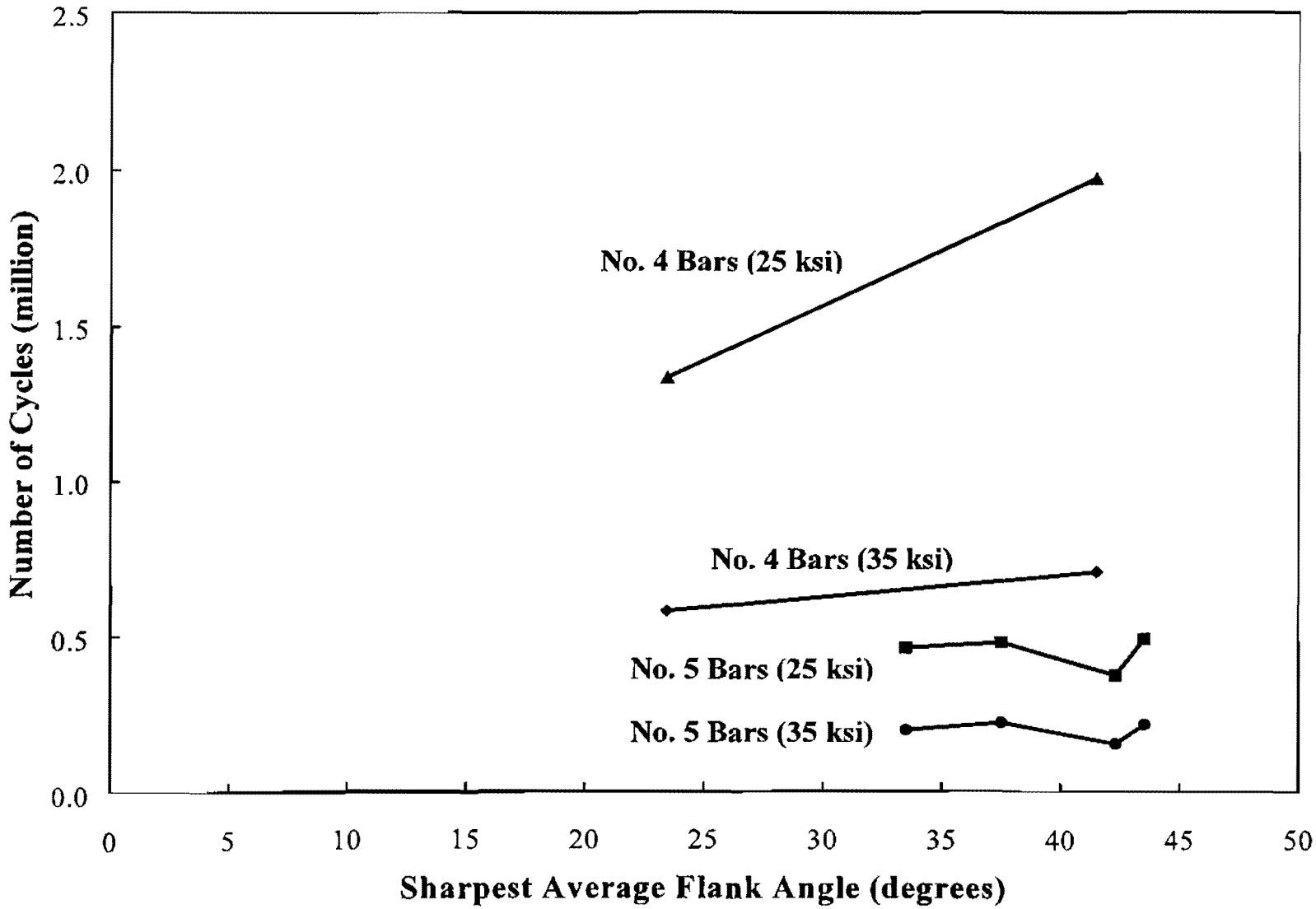

Fig. 3.4 Effect of the Sharpest Average Flank Angles

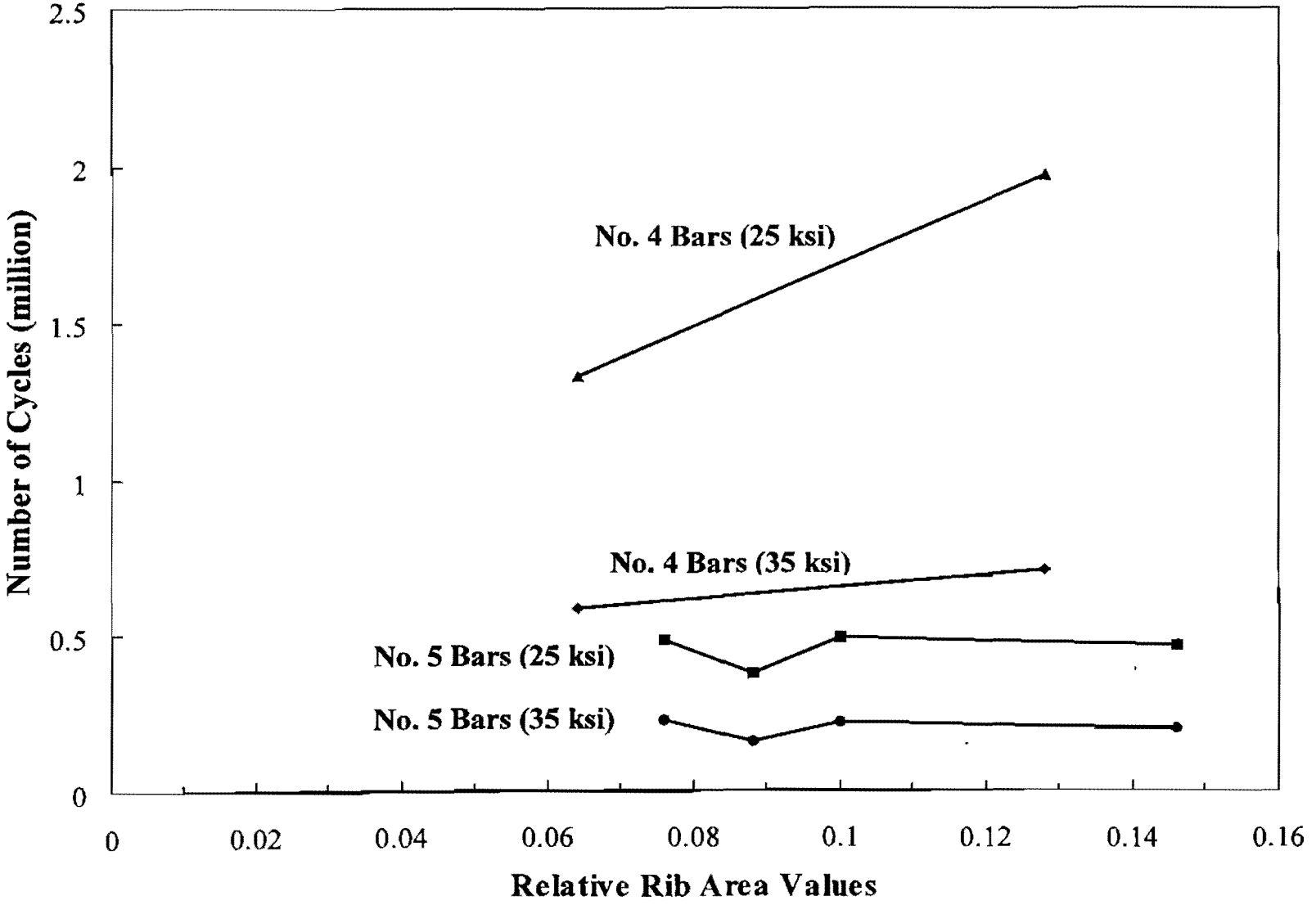

Fig. 3.5 Effect of Relative Rib Area (R_r) Values

APPENDIX

NOMENCLATURE

fatigue: the phenomenon of rupture of a material, when subjected to repeated loading, at a stress substantially less than the static strength.

fatigue strength: the greatest stress which can be sustained for a given number of load cycles without failure. For design purposes, the fatigue strength is usually defined as the stress *range* sustained without failure for a specified number of cycles.

stress range: the difference between the maximum stress and the minimum stress in a stress cycle, (S).

S-N curve: the curve reflecting the relationship between the stress range (S) and the number of load cycles (N).

relative rib area: ratio of projected rib area normal to bar axis to the product of the nominal bar perimeter and the center-to-center rib spacing.